VISUALIZING INTRA- AND EXTRACELLULAR VESICLES OF B CELLS USING EXPANSION MICROSCOPY

MARIA TARCZEWSKA

Master's thesis

University of Turku
Faculty of Medicine
Institute of Biomedicine
29.04.2023

Master's degree in Biomedical Imaging
Microscopy Techniques and Instrument Design

Credits: 20 ECTS

Supervisors:
Pieta Mattila, PhD, Docent
Saara Hämälistö, PhD

UNIVERSITY OF TURKU
Faculty of Medicine
Institute of Biomedicine

MARIA TARCZEWSKA: Visualizing intra- and extracellular vesicles of B cells using expansion microscopy

Master's thesis, 65 pp.
April 2023

Abstract

B lymphocytes (B cells) are a part of the adaptive immune system, where they are responsible for the production of antibodies against specific antigens. Upon antigen encounter, they become activated which alters their shape, size, and cytoskeleton. B cells release extracellular vesicles (EVs) that may help in antigen processing during activation. However, research data on the functions and characteristics of B cell EVs are scarce, and the content and function of these vesicles are largely unknown.

During B cell activation, vesicular populations such as lysosomes and endosomes traffic to the immune synapse where they have reported functions in antigen extraction and processing. Numerous proteins are found at the immune synapse and the role of many of them is unknown. Tetraspanins are known to play diverse roles in B cells. Here, the localization of tetraspanins CD63 and CD81 upon B cell activation was investigated using immunofluorescence microscopy (IF) and expansion microscopy (ExM). CD63 was shown to relocate to the perinuclear area of the Raji D1.3 cells upon B cell activation. CD81 was observed predominately in the cytoplasm and no changes in CD81 localization were observed.

The second part of the thesis focuses on imaging EVs using ExM. Studying vesicles is challenging due to their nanoscopic size. Here, ExM was implemented to study B-cell EVs. We show that ExM with in-gel suspended EVs allows for super-resolution imaging, although further data is required to verify the method's reliability. In the future, it can be used to study the morphology and content of EVs.

KEYWORDS: Expansion microscopy, B cell activation, EVs

List of Abbreviations

(p)MHC	(peptide) major histocompatibility complex
AFM	atomic force microscopy
AKT	protein kinase B
APC	antigen-presenting cell
BCA	bicinchoninic acid
BCR	B cell receptor
Btk	Bruton's tyrosine kinase
CryoEM	cryo-electron microscopy
DAPI	4′,6-diamidino-2-phenylindole
dSTORM	direct stochastic optical reconstruction microscopy
EBV	Epstein-Barr virus
ELISA	enzyme-linked immunosorbent assay
ERM	ezrin, radixin, moesin
ESCRT	endosomal sorting complexes required for transport
exRNA	extracellular RNA
FasL	Fas ligand
FCS	fetal calf serum
FoxO	forkhead box O
GS	gelation solution
IgM	Immunoglobulin M
ILVs	intraluminal vesicles
IS	immune synapse
ISEV	International Society for Extracellular Vesicles
ITAM	immunoreceptor tyrosine-based activation motif

Lyn	Lck/Yes novel tyrosine kinase
MBAm	N,N'-Methylenebisacrylamide
MFI	mean fluorescence intensity
MS	monomer solution
MVBs	multivesicular bodies
MVEs	multivesicular endosomes
NTA	nanoparticle tracking analysis
NVEPs	non-vesicular extracellular nanoparticles
PBS	phosphate-buffered saline
PEG	polyethylene glycol
PenStrep	penicillin-streptomycin
PFA	paraformaldehyde
PIP3	phosphatidylinositol-3,4,5-triphosphate
PLCγ2	phospholipase C gamma 2
PROSPR	protein organic solvent precipitation
ROI	region of interest
SEC	size exclusion chromatography
SEM	scanning electron microscopy
SLOs	secondary lymphoid organs
Syk	spleen tyrosine kinase
TCR	T cell receptor
TEM	transmission electron microscopy
UC	ultracentrifugation
WCL	whole cell lysate

LIST OF FIGURES

TABLE OF CONTENTS

1 LITERATURE REVIEW

1.1 THE IMMUNE SYSTEM

The human body is constantly exposed to a diversity of organisms that may pose a potential threat to it. These organisms can come into contact with our bodies by entering them from the external environment, for example, through inhalation or ingestion. Potential threats can also come directly from the skin and mucous membranes in our bodies. The lack of a proper defense system would allow pathogens to enter our bodies and replicate freely and infect the cells. To react against this, the immune system, composed of lymphoid organs, immune cells, humoral factors, and cytokines, constantly surveils each part of the human body [1]. The mechanism of action of the immune system is highly complex and still not fully understood.

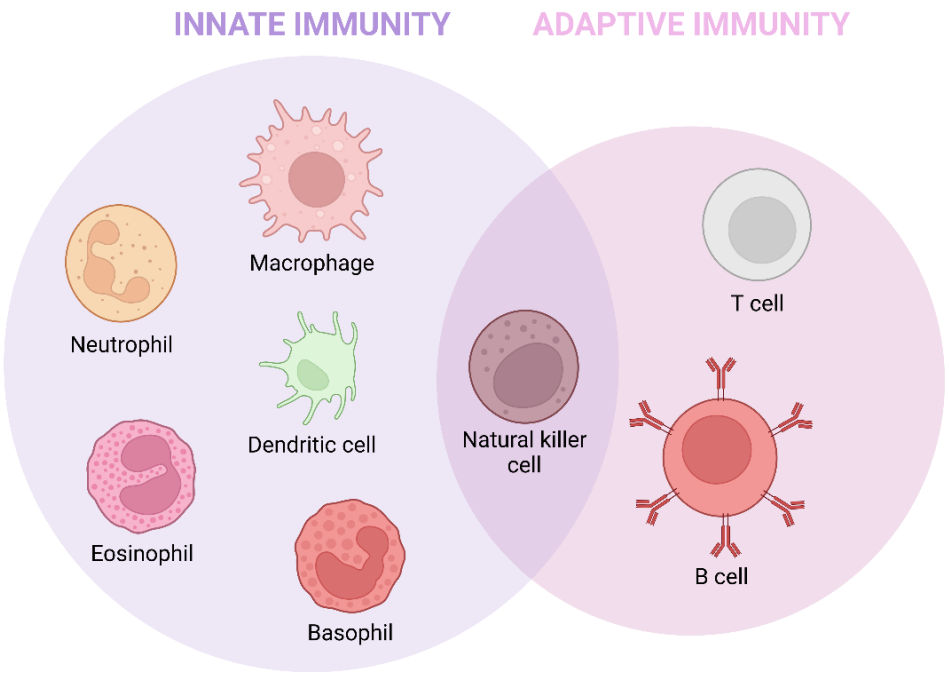

Figure 1 Cells of the innate and adaptive immune system. The immune system can be divided into adaptive and innate immunity. The innate immune system provides rapid responses against pathogens, while the adaptive immune system is characterized by higher specificity of the responses. The innate immune system includes cells such as macrophages, neutrophils dendritic cells, basophils, and eosinophils. The adaptive immune system includes B cells and T cells. Natural killer cells function at the interface of adaptive and innate immunity.

Cells of the immune system are heterogeneous and differ significantly in the functions they perform [Figure 1]. Just like other types of cells, immune cells express a variety of proteins on their cell membranes that differ between the cell types. Among the many proteins that are expressed, immune cell receptors, which interrogate the extracellular environment for potential threats such as infection or abnormal cell death, can be distinguished [2].

The immune system of vertebrates has traditionally been divided into innate and adaptive immune systems. Those two subsystems differ in speed and specificity of the immune response. Both of these systems are not mutually exclusive, but rather work together to effectively combat threats [3].

1.1.1 Innate Immune System

The innate immune system is a highly conserved and evolutionarily older form of immunity. Innate immunity is inborn and more universal than adaptive immunity. It is characterized by rapid responses against pathogens. Immune responses can be initiated within minutes or hours, but there is no immunological memory present, and the specificity of the immune responses is compromised. For the majority of organisms, it is the only line of host defense. The innate immune system aims to recognize and kill pathogens while sparing the host tissues. This goal is achieved using a combination of cellular and humoral elements. Innate immunity is non-specific and responds to molecular patterns shared between related pathogens [4], [5]. Defensive barriers that constitute the innate immune system can be physical, chemical, and microbiological, for instance, skin, mucus, and immune cells [1].

1.1.2 Adaptive Immune System

Adaptive immunity has evolved only in vertebrates as a mechanism for the recognition and elimination of pathogens. The main function of the adaptive immune system is to recognize specific foreign antigens and eliminate them [4]. The adaptive immune system provides antigen-specific responses that are carried out by B lymphocytes and T lymphocytes. The development of an adaptive immune response can take multiple days but is especially important when the innate immune system fails to eliminate the danger. The adaptive immune system maintains memory cells that allow for the presence of immunological memory, which enables faster responses to each subsequent encounter of the antigen [1]. Abnormal functioning of the adaptive immune system leads to the development of autoimmune diseases, where the immune system attacks host cells.

The specificity of adaptive immune responses is achieved through the process of somatic recombination. Developing B and T lymphocytes undergo the process of V(D)J recombination which highly diversifies the repertoire of the receptors that those cells can express. Thanks to this mechanism the cells can theoretically express receptors for every possible pathogen that an organism can encounter [6]. The receptors expressed on B cells are called B cell receptors (BCR), and those expressed on T cells are named T cell receptors (TCR).

The adaptive immune system can respond to pathogens using either a cell-mediated response or an antibody response. Antibody response is mediated by B cells that secrete antibodies thus preventing the spread of infections.

1.2 B LYMPHOCYTES

B lymphocytes, also known as B cells, are small (6-8 μm) white blood cells that in humans originate from hematopoietic stem cells [7]. Immature B cells develop in the bone marrow, where they undergo positive and negative selection to eliminate self-reactive cells. When they leave the bone marrow, they move to the secondary lymphoid organs (SLOs), such as the spleen, as mature B cells. B cells play a crucial role in humoral immune responses by producing antigen-specific antibodies upon antigen encounter. After maturation, B cells reside in SLOs through which they constantly circulate in search of antigens. Antigens are recognized through BCR, binding of which leads to B cell activation and differentiation into either memory B cells or antibody-secreting plasma cells [5], [8]–[10].

1.2.1 B cell activation

B cells are activated by foreign antigens which can be either membrane-bound or soluble. Multiple signaling cascades are activated upon antigen recognition which leads to B cell differentiation into either memory or antibody-secreting plasma cells. Membrane-bound antigens are considered to be a prevailing form of antigen presentation. *In-vivo,* B cells can encounter antigens that are bound to the plasma membrane of antigen-presenting cells (APCs). B cell encounter of membrane-bound antigen leads to the formation of the immune synapse (IS) which is a specialized intercellular contact site with the actin cytoskeleton and targeted vesicular movement being some of its integral components [11].

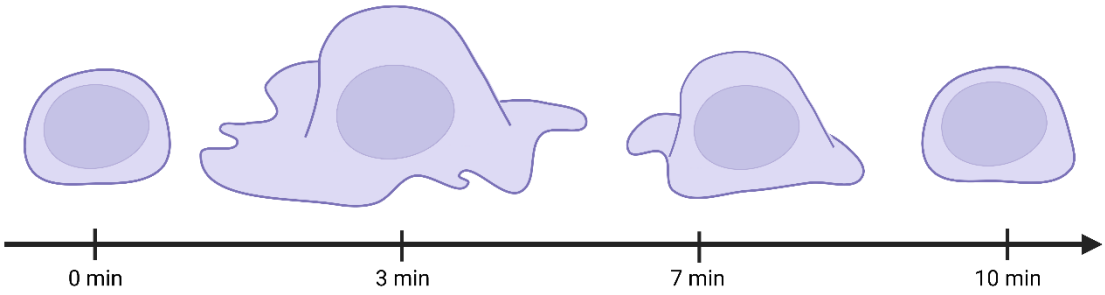

Figure 2 B cell spreading. Spreading response is characteristic of B cells upon antigen encounter. The cell maximizes the area of the antigen contact surface to then contract and collects the antigen into the central cluster. The time points presented on the timeline might differ between the cells.

B cell response to antigen recognition can be divided into two phases [Figure 2]. In around the first 4 min after the contact between the cell and the antigen, the cell flattens and

spreads, maximizing the surface area of the contact site with the antigen-bearing membrane. Then the cell starts to slowly contract, which can last for approximately 7 minutes [12]. In the contraction phase, the antigen is collected from a bigger membrane area into the central cluster.

Both normal and malignant B cells express BCR which is crucial for their functions. Although many events in BCR activation remain to be discovered, multiple downstream signaling components have been described. Among signaling pathway regulators, that are crucial for B cell function and development, Src-family kinases can be distinguished, as well as Bruton's tyrosine kinase (Btk), forkhead box O (FoxO), and AKT (protein kinase B). BCR conformational changes that are induced by antigen binding lead to the activation of Src kinases such as Lyn, Blk, Fyn, and Yes. Phosphorylated kinases then lead to the phosphorylation of downstream molecules such as Btk, which mediates signaling and survival in malignant B cells. Btk resides predominately in the cytoplasm but can be recruited to the cellular membrane upon phosphorylation. After BCR activation the signal is propagated by various signaling molecules. This leads to the phosphorylation of Btk by PIP3. Phosphorylated Btk (pBtk) then phosphorylates its downstream components such as PLCγ2, leading to the release of calcium from the endoplasmic reticulum into the cytoplasm. The release of calcium leads to the activation of transcription factors NF-κB and NFAT [13], [14]. Due to its role in BCR signaling, pBtk can be used as a marker of B cell activation. It has been identified as a protein signature for active BCR signaling next to pSyk and pLyn [15].

AKT is another key signaling molecule, which plays a role in promoting B cell growth and survival by inhibiting pro-apoptotic factors. The important AKT substrates are FoxO transcription factors. They regulate the expression of genes that are involved in B cell development and differentiation [14], [16].

1.3 EXTRACELLULAR VESICLES

Extracellular vesicles (EVs) are lipid bilayer-enclosed structures that cells secrete to communicate with each other [17], discard cellular debris, or transmit hormones in nerve synapses. Cells can exchange the EVs in an either autocrine, endocrine, or paracrine manner [18]. EV secretion is a conserved process that is present in all cells from bacteria to humans, where EVs are released from tissue types into body fluids. EVs can carry various signaling molecules such as proteins, lipids, or nucleic acids, over long or short

distances inside the organism. They are highly heterogeneous and can originate from different intracellular compartments [Figure 3].

Multiple ways to describe different EV subpopulations have been proposed. Based on their biogenesis, extracellular vesicles can be divided into exosomes and microvesicles. Exosomes originate from intraluminal vesicles (ILVs) and are secreted upon the fusion of multivesicular endosomes (MVEs) with the cell membrane. Microvesicles are generated by the outward budding of the plasma membrane. The nomenclature referring to specific types of EVs is not yet fully precise as different EVs often share similar features in terms of their morphology, sizes, and surface markers [19]. Next to exosomes and microvesicles, multiple EV subpopulations have been discovered such as migrasomes [20], exophers, secretory amphisomes, and autophagosomes [18]. Apart from EVs, extracellular space is also full of non-vesicular extracellular nanoparticles (NVEPs). Cells can release RNA and DNA together with lipoproteins in the form of NVEPs which lack lipid bilayer. NVEPs are in a similar size range to EVs and can be present in EV samples that were obtained using general methods such as size-exclusion chromatography or ultracentrifugation. It is however possible to distinguish between NVEPs and EVs based on their molecular composition. Different levels of lipids, nucleic acids, and proteins between EVs and NVEPs cause differences in their densities. For this reason, density gradient fractionation can be used to separate and purify EV samples from NVEPs [21].

In 2007 Valadi et al. discovered that exosomes can contain mRNA and microRNA and that the RNA content of the exosome can have a functional role in recipient cells [22]. This discovery boosted the field of EV research. Many new publications focused on extracellular RNA (exRNA), which is a term that was primarily used to describe RNA carried by exosomes [21]. Due to the possible functional roles of exosomal RNA, EVs have been extensively studied as potential biomarkers for diseases. EV studies are now clinically relevant for both the treatment and diagnosis of cancer as well as neurological, cardiovascular, and autoimmune diseases. EVs can carry pathological cargo, accelerate tumor growth, and promote metastasis [23]. Also, differences in the surface composition of EVs are relevant in their application as biomarkers. It has been shown that EVs derived from malignant cells differ in terms of their lipid composition from EVs derived from non-malignant cell lines [24]. Brzozowski et al. identified that EVs derived from prostate cancer cells had higher levels of certain lipids, including sphingomyelin and glycosphingolipids, compared to EVs from non-malignant prostate cells [25]. There is a potential for EVs to be used during cancer diagnosis and therapy [26]. Unraveling the

mechanisms underlying EV-mediated intercellular communication can lead to novel strategies in the diagnosis and therapy of different diseases, hence the increasing need for reliable tools and methods for EV research.

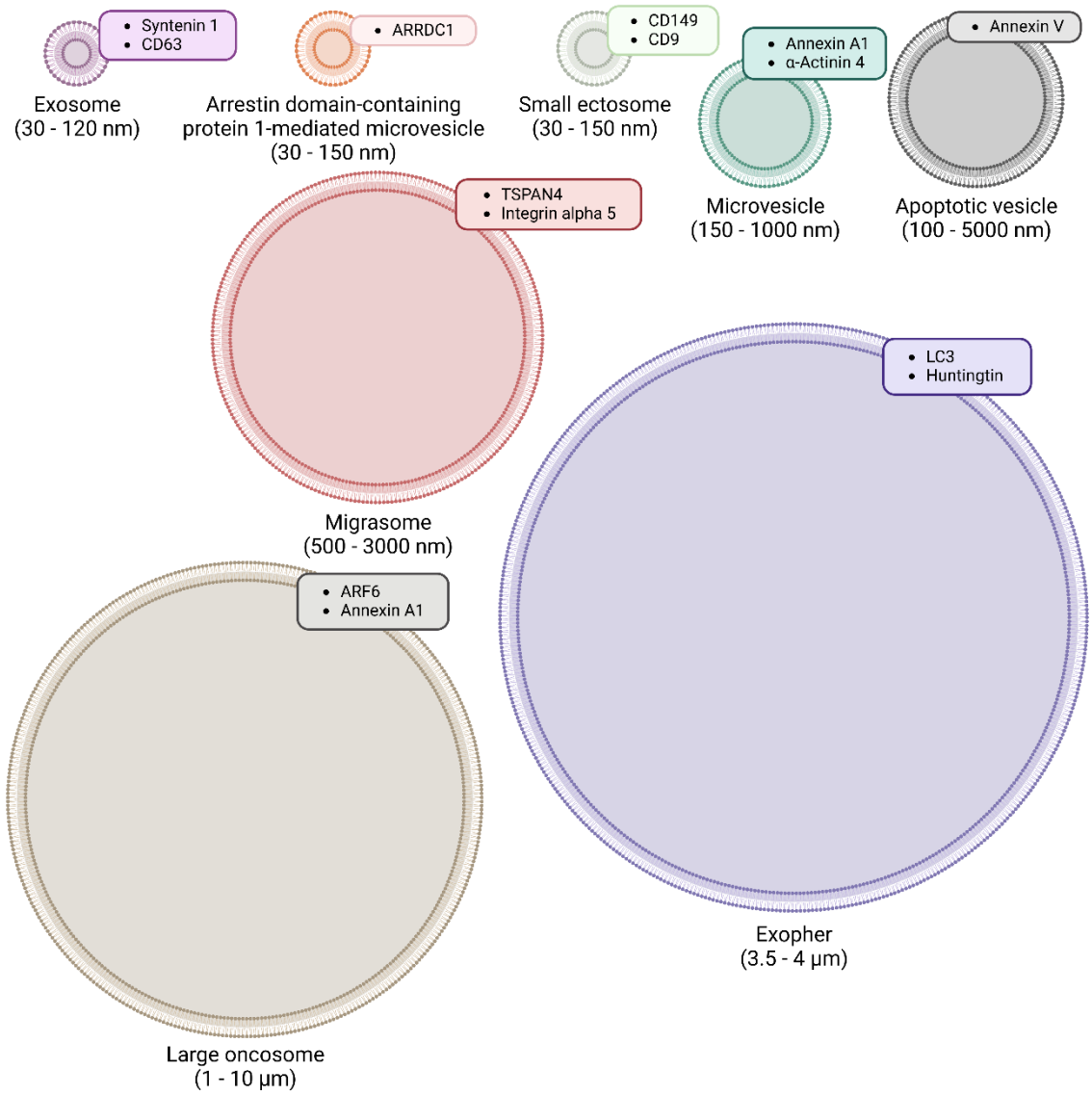

Figure 3 Types of EVs. Schematic representation of different EV types. EV population is highly heterogenous and with different EV subpopulations having overlapping sizes ranging from 30 nm to 5 µm. Exosomes originate from multivesicular endosomes. Arrestin domain-containing protein 1-mediated microvesicles, small ectosomes, microvesicles, and large oncosomes originate from ectosomes. Migrasomes originate from retraction fibers, apoptotic vesicles are released upon apoptosis and the origin of exophers still remains to be investigated. Each of the EV subtypes has its own unique characteristics. Example markers for each EV type are listed in the boxes next to EVs.

Although current EV isolation techniques allow for the separation based on their size and surface antigens, the distinction based on the site of their biogenesis is still not possible [18]. One of the features that can be characteristic of different EV populations is the composition of their surface proteins, which will be described in more detail in the following chapter.

1.3.1 The surface composition of EVs

Depending on the type of vesicles and their biogenesis as well as the cell that secretes them and multiple other factors, the surface composition of EVs as well as their cargo varies. The surface of EVs is highly interactive and dynamic and its composition contributes to the process of interaction between EVs, the extracellular environment, and other cells. Surface proteins of EVs are used to target recipient cells and regulate EV intake [27]. EV surface composition can also reflect the parent cells as well as their intracellular origin. It can be characteristic of a particular type of EV and therefore be used in their selective isolation and identification [24].

The surface of EVs is composed of molecules such as proteins, lipids, nucleic acid, and glycans. The distribution of lipids in EV membranes is unique and distinct from the cellular membrane composition with cholesterol and sphingolipids being the two major components. Surface molecules of EVs include tetraspanins, MHC, cell adhesion molecules, integrins, and different types of receptors [24]. Tetraspanin proteins such as CD9, CD63, and CD81 are commonly used as EV markers [28] and will be described in more detail in Chapter 1.3.2.

Different sets of proteins that are characteristic of various EVs subtypes have been identified. For instance, exosomes can be characterized by the presence of ESCRT protein and Alix, TSG101, HSC70, and HSP90β, which are ESCRT accessory proteins. This is due to their formation, in multivesicular bodies (MVBs), which is regulated by ESCRT [29]. The proteomic study conducted on different human cell lines showed the presence of typically used exosome markers such as MHC, flotillin, and heat-shock 70-kDa proteins in the EVs samples, although they were not enriched in EVs smaller than 220 nm [28]. Also, tetraspanins CD9, CD63, and CD81, which are classically used as exosome markers, have been shown to be present in other types of EVs. Tetraspanins CD63 and CD9 are specific to EV subpopulations and might not be present in all of the EVs. Kowal et al. suggest that the presence of vesicles in the sample can be demonstrated by the detection of any cell membrane protein that is normally present on the surface of the cell from which the EVs were derived, such as, for example, MHC I or II [28].

One protein, relevant to the immune cells, that can be found in EVs is cathepsin S [30]. Cathepsin S is a protein belonging to the family of lysosomal cysteine cathepsin proteases. It's highly expressed in immune cells and participates in MHC II antigen presentation and antigen processing [31], [32]. It is involved in the endo-lysosomal pathway where it contributes to the lysosomal degradation of proteins in acidic lysosomes and it has also

been shown to participate in intra- and extracellular substrate cleavage [33]. Like other members of the cysteine cathepsins family, cathepsin S is a membrane protein and can be secreted inside lysosomal or endosomal vesicles, therefore its presence in the isolated sample indicates the vesicular nature of studied material.

New molecules are frequently added to the list of EV markers. An example of such protein is ezrin. Ezrin belongs to the ERM (ezrin, radixin, moesin) group of adaptor proteins that link the actin cytoskeleton with the plasma membrane and participate in cell division, cell migration, and invasion. ERM proteins are regulated by sphingolipids which are abundant on the EV surface. They are involved in processes that require the change of the plasma membrane shape such as endocytosis, exocytosis, filopodia formation, or cellular trafficking. ERM proteins are considered to be essential in facilitating signal transduction between the cell and extracellular matrix [34]. Due to ERM proteins association with cellular membranes and exocytosis ezrin can be used as an indicator of EV presence in the isolated sample.

1.3.2 Tetraspanins

Tetraspanins are a family of small membrane proteins with four transmembrane domains [35]. They are synthesized in the endoplasmic reticulum, are present in all cell types and their architecture is highly conserved. Proteins belonging to this family share a characteristic structure, with four transmembrane helixes and a cholesterol-binding pocket that regulates the switch between the open and closed tetraspanin conformation [Figure 4]. Tetraspanins are often found in curved membrane regions such as endosomes, extracellular vesicles, or filopodia. They are commonly used as EV markers, especially tetraspanins CD9, CD63, and CD81, due to their relative enrichment in the EVs [35], [36]. Tetraspanins participate in multiple cellular processes such as the regulation of protein trafficking, cell signaling, and membrane fusion, and take part in cell adhesion, motility, and regulation of cell morphology [37], [38].

Tetraspanins can also be found inside the cell, where they can either accumulate or travel between the plasma membrane and subcellular localisations. For instance, CD63 is localized in late endosomal compartments as it mediates exosomal biogenesis via ESCRT [36]. A small fraction of CD63 always resides on the cell surface. CD63 present on the plasma membrane can be endocytosed via clathrin-coated pits [Figure 4]. Caveolae might also contribute to the endocytosis of CD63. After endocytosis, CD63 can then be enriched and incorporated into ILVs both in early endosomes and in multivesicular bodies MVBs, with the help of the ESCRT machinery. From early endosomes, CD63 is transported into

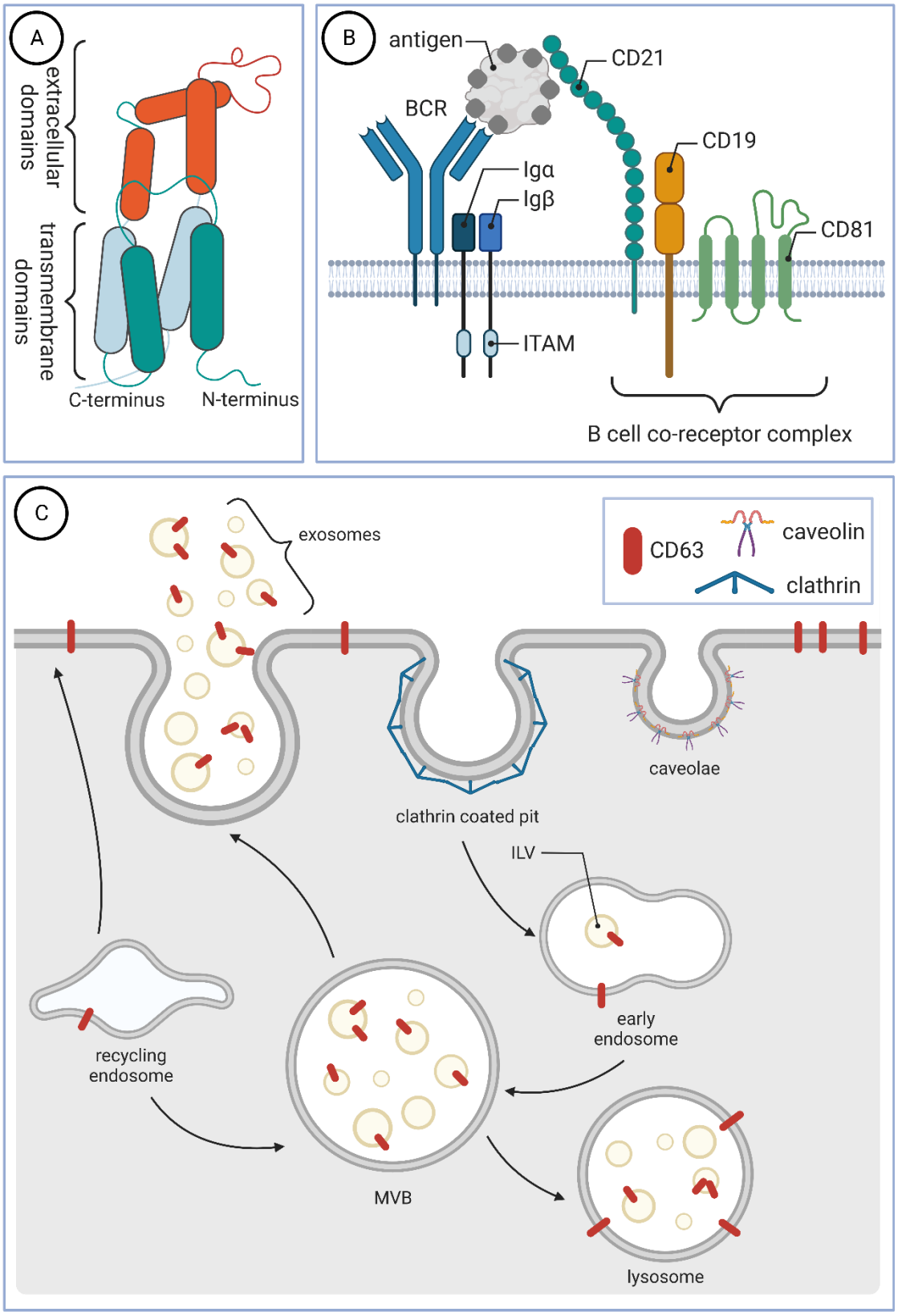

Figure 4 Tetraspanins in a nutshell. (A) Schematic structure of tetraspanin. The tetraspanin molecule is composed of four transmembrane domains and three extracellular domains. Between transmembrane domains, there is a cholesterol-binding pocket that regulates the switch between open and closed conformation (**B)** The role of tetraspanins in B cell activation. Tetraspanins CD19/CD81/CD21 create a co-receptor complex present on a B cell surface in the proximity of BCR. It's involved in B cell activation by amplifying the BCR signaling. (**C)** Intracellular trafficking of CD63. Tetraspanin CD63 mediates exosomal biogenesis. It can be localized on the plasma membrane and endocytosed. CD63 present on early endosomes can be released on EVs into the extracellular space or remain inside the cell on lysosomal membranes. The schematic drawing doesn't reflect the actual position of CD63 in the membrane, which is not well known. Adapted from [35].

MVBs. CD63 can be released from MVBs to extracellular space on exosomes or stay on the lysosomal surface when MVBs mature or fuse with lysosomes [39]. Apart from CD63, other tetraspanins such as CD9 and CD81 are also involved in sorting the cargo into the MVBs and ILVs. Through this process, they are involved in sorting the EV cargo [36].

Several tetraspanins have been shown to have specific functions in B cells. It has been shown that the depletion of CD63 in B cells increases the secretion of exosomes [40]. The co-receptor complex CD19/CD81/CD21 is crucial for B cell development and maturation. It amplifies the BCR signaling which then leads to the adaptive immune response and antibody secretion [41]. CD81 is present at the IS of both B cells and T cells. It has been reported to be engaged in B cell signaling where it induces the activation of kinases such as Syk. It is also known to facilitate the connection to the actin cytoskeleton [42]. The CD81-containing tetraspanin network present in B cells has been shown to play a role in regulating the diffusion of CD19. In BCR signaling induced upon the disruption of the actin cytoskeleton, CD81 regulates the mobility of CD19. In antigen-independent BCR signaling the presence of CD19 is required for signal propagation [43].

Due to their role in vesicle trafficking, tetraspanins such as CD63 are good markers for the microscopy visualization of vesicular structures inside the cell when combined with techniques such as immunofluorescence microscopy.

1.3.3 Extracellular vesicles of B cells

Among numerous other functions in the organism, EVs have several roles related to the immune system. By mediating the communication between different immune cells they can modulate immune responses [44]. Immune cell-derived EVs are also involved in a multitude of physiological processes and different diseases. EVs participate in antigen transfer to APCs and carry immuno-modulatory cytokines. The unique immunological conditions of pregnancy are associated with an increased level of circulating EVs which raises while the pregnancy progresses [45]. The release of EVs is also associated with B cell activation. B cells can secrete vesicles containing MHC II, which then induce T-cell responses [46]. It has been shown that activated B cells secrete in EVs a significant amount of their peptide-MHC II (pMHC II), which was previously present on their plasm membrane. As activated B cells were observed to degrade roughly half of their pMHC II, this mechanism might prevent an intracellular degradation of a part of their pMHC II [47].

CD24 is a cell adhesion protein expressed by various cell types, including immune cells. It is known to be involved in tumorigenesis, with surface expression of CD24 on

malignant cells being associated with changes in several oncogenic signaling pathways [48]. It has been shown that the stimulation of B cells with CD24 triggers the release of CD24-carrying plasma-membrane-derived vesicles [49]. The vesicles, that B cells secrete upon stimulation with CD24 or IgM, carry lipids, CD24 and IgM to the recipient cells, and can also carry a functional BCR [50]. The EV release from B cells can be induced by different cytokine activation signals [51].

The studies done on B cell-secreted EVs show that different established B cell lymphoma cell lines differ in terms of the proteins expressed on the EVs that they secrete. Different B cell-derived EVs were shown to express CD19, CD20, CD24, CD37, and HLA-DR in addition to CD81 and CD63 described in Chapter 1.3.2. The expression of classical EVs tetraspanin markers CD9, CD63, and CD81 differs between different B lymphoma cell lines, and in many of them CD9 is not expressed [52].

It has been shown that B cell EVs, derived from patients with birch pollen allergy, are capable of presenting allergen-derived peptides to T cells, stimulating their proliferation and the production of TH-2-like cytokine [53]. Some B cells express Fas ligand (FasL), which is an apoptosis-inducing protein. It has been observed that the B cells immortalized with Epstein-Barr virus (EBV) release exosomes that contain FasL and MHC II, which are capable of killing antigen-specific T helper cells, which play an important role in immune tolerance development [54].

Studies suggest that the capture of B cell-derived EVs is facilitated by the presence of sialic acid expressed on their surface, which is recognized by CD169 on the plasma membrane of recipient cells. These EVs have been observed to localize in macrophages present in the spleen and lymph nodes of mice. [55]. Although EVs have numerous important functions in the immune system, their outcome, after entering recipient cells, might not always be positive. It has been reported that the CD19 positive B cell-derived EVs can inhibit CD8 positive T cell responses and therefore adversely affect the cancer treatment [51].

Multiple studies have been conducted that broadened our understanding of the roles of B cell-derived EVs, their functions, and molecular composition. However, similar to other cell types, the B-cell EV population is highly heterogenous and requires further characterization. To the best of our knowledge, the differences in EV secretion as well as their molecular composition between activated and non-activated B cells were not yet studied. The understanding of the effector functions carried out by EVs can deepen our

knowledge of how immune responses are modulated and potentially be used as a novel therapeutic tool. This implies a need for further studies on B cell-derived EVs as well as the value of novel tools and methods that can be used in the field of EV research.

1.3.4 Current approaches to EVs studies

Recently, EVs have become more extensively studied. However, it has been suggested that there is a lack of appropriate nomenclature and methodology in EV studies and that there is a rising need for standards and controls in the existing methods [18]. Existing EV purification methods are limited and are always a trade-off between the yield, purity, and heterogeneity of isolated EVs. Many of the methods rely on the characterization of a larger EV population at a time and therefore do not focus on their heterogeneity.

EV studies can be carried out either *in-vitro* or *in-vivo*, in cell cultures, tissues, or animals as well as on isolated EVs. The chosen method of EV isolation can impact the results of the studies as it has been shown that EVs from the same source show different proteomic profiles based on their isolation method. The fractions of EVs that can be obtained differ in their homogeneity depending on the method of choice making it hard to compare the results between different proteomic studies [56].

Commonly used approaches for EV isolation include ultracentrifugation (UC) [57], density gradient centrifugation, filtration, and size-exclusion chromatography (SEC) [56]. Those approaches can result in the isolation of different EV subpopulations as well as different level of sample contamination. A comparative study of different EV isolation methods has shown that both UC and UC combined with SEC result in similar EVs yield, however, the yield in the EVs isolation by precipitation was around 4 times higher. The research showed that due to the overlap of size and density of EVs with different non-EV particles no 100% pure EVs sample can be obtained. Both sample preparation and EV separation protocols also influence the purity of EVs samples. Choosing the appropriate method for EVs isolation is also dependent on the sample type [58]. EVs can be isolated for instance from cell culture media, serum, urine etc. All of those samples differ in terms of their physical properties and present contaminations which affects the difficulty of EVs isolation and the performance of different methods.

SEC has been shown to be the most effective at removing soluble plasma proteins during EVs isolation compared to the precipitation with polyethylene glycol (PEG) and protein organic solvent precipitation (PROSPR). The research showed that, as opposed to PEG and PROSPR, SEC does not alter the sizes and other characteristics of EVs. The studies

demonstrate that SEC maintains the structure and conformation of EVs, therefore has the potential to be used as a tool for clinical applications and biomarker discovery [59].

The International Society for Extracellular Vesicles (ISEV) proposes minimal criteria for EV characterization. Proteins commonly found in EVs are usually not EV-specific but only enriched in EVs. Because of that ISEV suggests that the presence of components that are not expected to be found in EVs is also checked using methods such as Western blot or flow cytometry. What is also important is that the process of EV separation should not result in cell disruption. Disrupting the cells could result in the presence of intracellular vesicles in the sample and therefore affect its purity [60].

The isolation process might affect the structure of EVs. Some of the more fragile EV components like branched glycans can be destroyed during the isolation process [61]. Another issue that might occur during the process of EV isolation is the presence of lipoprotein and ultra-low-density lipoprotein contaminants especially when EVs are being isolated from the plasma using ultracentrifugation [62]. Due to common interactions between lipoproteins and EV surfaces as well as their overlapping densities and sizes co-isolation commonly occurs. This contamination can affect downstream EV isolate applications, especially lipidomics, and particle counting [24]. Van Deun et al. addressed this issue by developing a dual-moded chromatography, which combines SEC with cation exchange, as a method that can deplete lipoproteins from EVs isolated from plasma. This approach was shown to improve EV identification during image analysis as well as EV protein analysis [63].

Physical characterization of EVs can be done using microscopy-based methods, such as SEM, TEM, CryoEM, or AFM, as well as other approaches like NTA or dynamic light scattering. EVs can also be analyzed in terms of their protein content with methods such as western blotting, ELISA, mass spectrometry, and many others [64]. The nanometer size range of the most widely studied EV populations hinders the usage of diffraction-limited microscopes for such studies [18]. Methods such as SEM, TEM, or AFM require specialized equipment and sample preparation protocol. Also, the throughput of such methods is low.

In recent years several labeling strategies have been developed to enable EV imaging in fixed samples and *in-vivo* tracking. Choosing appropriate dyes allows focusing on different aspects of EV subpopulations such as their biogenesis, uptake, cargo transfer, biodistribution, etc [61]. Lipid dyes are widely used for EV studies and PKH lipid dyes

were commonly used for membrane staining also in EVs. PKH-stained EV samples were shown to contain non-EV fluorescent structures. Further studies carried out on exosomes derived from a lymphoblastoid B cell line that included confocal microscopy imaging showed that ultracentrifugation-based exosome staining generates PKH-positive particles, in a similar size range to PKH-labeled vesicles, which are almost indistinguishable from EVs. Only 11% of the PKH-positive particles were exosomes while the rest consisted of nanoparticles. In sucrose-based staining, the number of exosomes constituted 34% of the sample. The study also reported the uptake of PKH-positive non-EV particles by primary astrocytes [65]. Recently, MemGlow has been proposed as an alternative for EV staining. It belongs to the MemBright probes family, which has been shown to be less prone to aggregate. MemBright is expected to form soluble aggregates in aqueous media, however, the aggregates will disassemble in lipid membranes [61], [66]. Although lipid dyes can be applied directly to the cells in order to isolate already labeled EVs it is not known if the labeling might interfere with EV biogenesis and uptake.

Another approach for labeling EVs are genetically encoded reporters. Fluorescent proteins expressed in the cytosol can then be transported into the lumen of EVs allowing for distinguishing them based on their cargo. They also enable the usage of imaging techniques such as photoactivation or photoswitching. It is also possible to target the surface protein of EVs with fluorescently labeled antibodies [61].

The limitations of current approaches to EV studies can have an impact on the results of scientific studies. Although methods such as SEC or ultracentrifugation are frequently employed, they may not provide a complete picture of EV populations. There is an increasing need for defining markers specific to different EV subpopulations. In recent years new methods are being developed that aim to improve the current approaches to EV isolation and purification making EV studies more reliable. Advances in imaging techniques, especially super-resolution offer promising possibilities to visualize EVs and study their conformation and composition. Currently used imaging modalities, such as electron microscopy, provide high resolution, however, the ability to visualize the molecules of choice by e.g. immunolabelling is limited. Using fluorescence microscopy could provide new information on EV composition, however, the resolution of a standard fluorescent or confocal microscope is not sufficient for EV studies.

1.4 EXPANSION MICROSCOPY

Light microscopy aims to visualize the details of the specimen that cannot be seen with the naked eye by creating an optically magnified image of the sample. To achieve this the light travels through the set of lenses and other parts that constitute the light path to produce a magnified image of the specimen at the end [67]. The resolution of a light microscope is restricted by the diffraction limit that was described by Ernst Abbe in 1873. According to the Abbe formula, the diffraction limit of an optical system is proportional to the wavelength of the incident light and inversely proportional to twice the numerical aperture of the objective, which is the measure of the range of incident light angles that an objective can collect [68]. Due to an increasing need for imaging subcellular processes with higher resolution than one of the conventional light microscopes, superresolution techniques are being developed that aim to overcome the Abbe resolution limit.

Superresolution microscopy techniques allow to resolve up to ~10 nm, however, they require expensive specialized equipment and fluorescent probes, and often their acquisition times are slower compared to e.g. standard confocal microscopy [69]. They are based on fluorescence microscopy setups, but the novel approaches to fluorophores excitation and fluorescent light detection allow us to lower the resolution limit of those microscopes down to the nanometer range [70]. Expansion microscopy differs from other superresolution modalities as the aim is to physically magnify the sample to enable subdiffraction imaging. It is compatible with the majority of standard fluorescent probes and samples can be imaged on standard fluorescence microscopes.

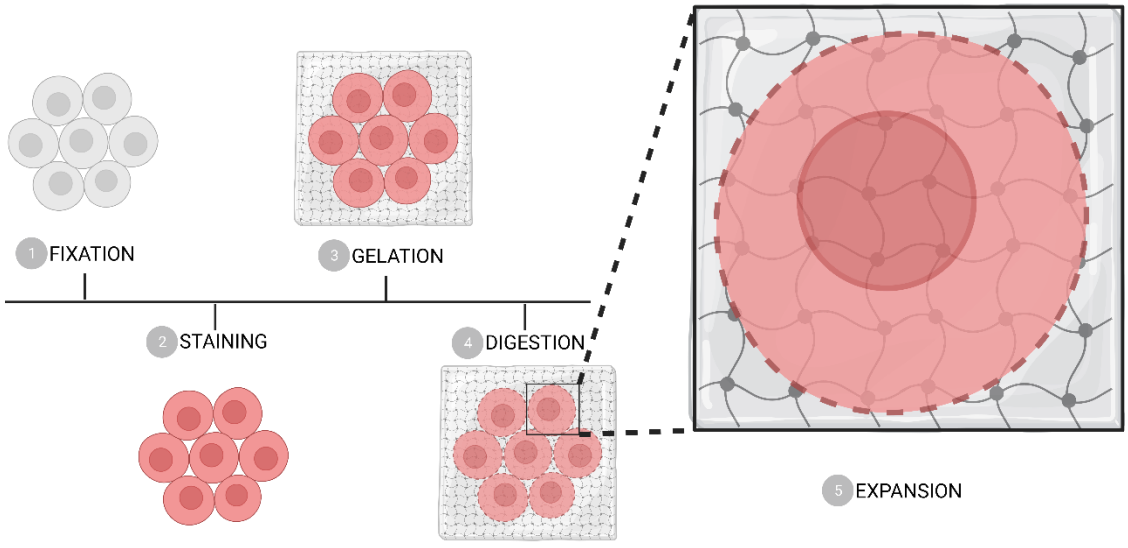

Figure 5 Schematic diagram of generalized workflow for expansion microscopy. First, samples are fixed and stained. This is followed by the synthesis of gel meshwork in the sample, where the samples become anchored to the gel. The gel is then subjected to proteolytic digestion to homogenize its mechanical properties. The last step is gel expansion by immersing it in water. This can result in up to ten-fold expansion of the samples.

Expansion microscopy was first proposed by Chen et al. in 2015 as a sample preparation technique that allows superresolution imaging to be performed on diffraction-limited microscopes [71]. In the originally proposed method, fluorescent labels were first anchored to the biomolecules of interest and then covalently attached to the polymer network. As the gel expanded the distance between the labels was increasing isotropically making it possible to optically resolve labels that were located closer than the diffraction limit before the expansion. This method required the usage of tri-functional custom fluorescent labels containing fluorophore, oligonucleotide, and methacryloyl group [71], [72]. The method proposed by Chen et al. did not preserve the proteins present in the sample and required the preparation of custom fluorescence labels. To resolve this issue Tillberg et al. developed a variant of expansion microscopy called protein-retention expansion microscopy (proExM) which allows for anchoring the proteins from the sample into the swellable polymer network. This method is now the most commonly used in the majority of laboratories as it allows to use commercially available fluorescent labels. Native proteins are anchored in the gel using cross-linking molecules and can be then stained both in the expanded state and before the expansion [73].

In the proExM protocol the samples can be prepared like for standard immunofluorescence microscopy and then incubated in acryloyl-X (AcX) which modifies the amines present in the proteins so that the proteins can be incorporated into the gel. Then the gel meshwork is synthesized in the sample followed by the proteolytic digestion of the gel which homogenizes the mechanical properties of the gel enabling uniform expansion. The sample can also be labeled post-expansion which may prevent the fluorescence bleaching or quenching that can be caused by the polymerization reaction. The final step of the sample preparation protocol is the expansion by immersing the gel in water which allows for the size increase of the gel to up to ten-fold. Osmotic force drives the water diffusion into the polyelectrolyte gel which causes gel swelling. The expanded gel consists mostly of water thereby it is transparent and index-matched with water. The high content of water in the expanded gel facilitates light transmission through the sample and allows for using faster imaging modalities, especially in thick samples [74], [75].

1.4.1 Applications of Expansion Microscopy

Since its development in 2015, expansion microscopy has been increasingly used in many laboratories worldwide. Chen et al. in their ExM discovery paper applied their technique for imaging microtubules in fixed HEK293 cells, clathrin-coated pits, and fixed brain

tissue slices [71]. Until now expansion microscopy protocol has been optimized for studying a wide selection of different biological specimens. Starting from thicker biological samples ExM is applied for studying a wide range of human tissue types such as the pancreas, colon, kidney, breast, liver, and lung [75]. It has also been used for vasculature and coronary vessels in heart tissue slices and whole-mount vasculature [76]. The popularity of the expansion microscopy technique increases in brain tissue studies. It has been used in neuroscience for imaging synapses, synaptic contacts, and subsynaptic architecture, studying neuronal connections, and studying neurological diseases [77]. It has also been optimized for studying clinical tissue samples with paraffin-embedded, hematoxylin and eosin-stained samples, and fresh-frozen thin-sliced samples in a method called expansion pathology [78]. Expansion microscopy is also a great tool for studying cell ultrastructure and has been successfully implemented for studying different fluorescent-labeled proteins and RNAs inside the cell. The example studies employing this technique investigated cellular organelles and organelle contacts [79], as well as cytoskeleton e.g. in neuronal cells [80]. ExM is also compatible with RNA and DNA studies as it is possible to covalently attach those molecules to the polyelectrolyte gel using a molecule linker [75], [81]. In the area of immunology, expansion microscopy has recently been used for studying nuclear structure in neutrophils and neutrophil extracellular traps [82]. It has been used for centrosomes and cilia studies [83]. Many other studies, that are not mentioned in the above summary, have utilized expansion microscopy, however, to the best of our knowledge the expansion microscopy technique has not yet been implemented for studying extracellular vesicles.

2 AIMS AND HYPOTHESIS

The aims of the thesis are:

1. To investigate the differences in localization of tetraspanins CD63 and CD81 in activated and non-activated B cells using immunofluorescence microscopy
2. To implement expansion microscopy for better visualization of intra- and extracellular vesicles of B cells

Hypothesis:

1. B cell activation induces changes in the tetraspanin localization
2. Expansion microscopy can be optimized to be used in EVs studies, providing a better understanding of the molecular organization of these vesicles

3 MATERIALS AND METHODS

3.1 REAGENTS AND BUFFERS

This chapter provides a list of all the antibodies, reagents, and buffers used throughout the course of this thesis, which are shown in Table 1 and Table 2 respectively.

Table 1 Antibodies and reagents. ExM – Expansion Microscopy. IF – Immunofluorescence Microscopy. SEC – Size Exclusion Chromatography. WB – Western Blot.

Name	Company	Catalog number	Application
4–15% Mini-PROTEAN TGX Precast Protein Gels, 10-well, 50 µl	BioRad	#4561084	WB
4x Laemmli Sample Buffer	BioRad	#1610747	WB
Acrylamide, PlusOne for PAGE	Cytiva	17-1302-01	ExM
Acryloyl-X	Fisher Scientific	A20770	ExM
ActinExM 561	Chrometra		ExM
AffiniPure F(ab')2 Fragment Donkey Anti-Mouse IgM, µ Chain Specific	Jackson ImmunoResearch	715-006-020	IF
AffiniPure F(ab')2 Fragment Goat Anti-Human IgM, Fc5µ Fragment Specific	Jackson ImmunoResearch	109-006-129	IF
Alexa Fluor 555 Phalloidin	Fisher Scientific	A34055	IF
Amicon Ultra-15 Centrifugal Filter Units	Millipore	UFC903024	SEC
Ammonium Persulfate (APS)	Millipore	2300-OP	ExM
Anti-CD81 antibody [M38]	Abcam	ab79559	WB
Anti-CTSS / Cathepsin S Antibody IHC-plus	LSBio	LS-B2550	WB
Anti-LAMP1−Cy3	Sigma-Aldrich	L0419	ExM
Bovine Serum Albumin Lyophilised pH ~7	Biowest	P6154-500GR	IF
CD63-mIgG1	DSHB	H5C6-s	IF
Cell-Tak™ Cell and Tissue Adhesive	Corning	354240	IF
DAPI (4',6-Diamidino-2-Phenylindole, Dihydrochloride)	Invitrogen	D1306	IF, ExM

Epredia PTFE Diagnostic Slides	Fisher Scientific	10028210	IF
Ezrin Antibody	Cell Signaling	#3145	WB
Fetal Bovine Serum, exosome-depleted, One Shot format	Fisher Scientific	A2720803	SEC, IF
Fibronectin	Sigma-Aldrich	F4759-2MG	IF
Fluoromount-G	Southern Biotech	0100-01	IF
Fluoromount-G containing DAPI	Fisher Scientific	00495952	IF
GAPDH Monoclonal antibody	Proteintech	60004-1-Ig	WB
Goat anti-Mouse IgG1 Cross-Adsorbed Secondary Antibody, Alexa Fluor™ 488	Invitrogen	# A-21121	IF, ExM
Goat anti-Mouse IgG1 Cross-Adsorbed Secondary Antibody, Alexa Fluor™ 555	Invitrogen	# A-21127	IF, ExM
HyClone RPMI 1640 medium	Cytiva	SH30027.01	Cell culture
Immobilon Western Chemiluminescent HRP Substrate	Millipore	WBKLS0500	WB
MembraneExM 561	Chrometra		ExM
MemGlow™ 488	Cytoskeleton	MG01-02	IF, ExM
Microcon Microconcentrators 10	Amicon	42407	SEC
N,N'-Methylenebisacrylamide	Sigma-Aldrich	M7279-25G	ExM
NNN'N'-Tetramethyl-ethylene diamine >=99% (TMEDA)	Fisher Scientific	10549960	ExM
Phospho-Btk (Tyr223) Antibody	Cell Signaling	#5082	WB
Polyclonal Goat anti-Human CD63 Antibody	LSBio	LS-C204227	WB
Poly-L-Lysine Solution	Santa Cruz	5988-63-0	ExM
Prestained protein marker	Proteintech	PL00001	WB
qEV1 / 35 nm Column	Izon	IC1-35	SEC
Sodium acrylate	AK Scientific	7446-81-3	ExM
Trans-Blot Turbo Mini 0.2 µm Nitrocellulose Transfer Packs	BioRad	#1704158	WB
Triton™ X-100	Sigma-Aldrich	9036-19-5	IF, ExM
TWEEN® 20	Sigma-Aldrich	9005-64-5	IF, ExM

Table 2 Buffers and solutions. ExM – Expansion Microscopy. IF – Immunofluorescence Microscopy. WB – Western Blot.

Buffers and solutions	Composition	Application
Blocking buffer	5% donkey serum in PBS	IF, ExM
Disruption buffer	5% SDS, 200 mM NaCl, 50 mM Tris in MQ	ExM
Monomer solution	1.1M sodium acrylate, 2.0 M acrylamide, 90 μg/ml MBAm in PBS	ExM
Permeabilization buffer	0.3% Triton X100 or 0.5% Tween 20 in PBS	IF, ExM
TBS-t (TBS-tween)	0.05% Tween 20 in TBS	WB

3.2 Cells

Expriments were done on BJAB and Raji D1.3 cell lines. BJAB is an EBV-negative lymphoblastoid cell line established from an African Burkitt's lymphoma [84]. BJAB cells were maintained in complete RPMI with 20% FCS, 1% PenStrep, and 1% L-glutamine. Raji is Burkitt's lymphoma cell line established in 1967 [85]. Raji D1.3 is a subclone of the Raji cell line that expresses the D1.3 IgM – BCRl. Raji D1.3 cells were maintained in complete RPMI with 10% FCS, 1% PenStrep, and 1% L-glutamine.

3.3 Cell activation

Cells were activated using either soluble or membrane-bound activation. These two activation modes are thought to reflect the antigen binding in the body fluids and on the surface of a solid tissue or cell, respectively. Soluble activation of BJAB cells was done by adding 10 μg/ml anti-human IgM $F(ab)_2$ to the cell culture medium. For Raji D1.3 cells, which express a transgenic hen egg lysozyme (HEL)-specific BCR, 10 μg/ml anti-mouse, IgM $F(ab)_2$ was used. Following the addition of anti-IgM, cells were incubated at 37°C in 5% CO_2 for 15 or 30 minutes before the subsequent sample handling.

Membrane-bound activation was done by coating twelve-well PTFE diagnostic slides or microscope glass coverslips by submerging them in 10 μg/ml of anti-human IgM $F(ab)_2$ or anti-mouse IgM $F(ab)_2$ in PBS, for BJAB and Raji D1.3 cells respectively. Slides/coverslips were incubated at 37°C degrees for 45 minutes and washed with PBS. Cells were then seeded on coated slides/coverslips and incubated at 37°C in 5% CO_2 for 15 minutes.

3.4 IMMUNOFLUORESCENCE MICROSCOPY SAMPLE PREPARATION

3.4.1 Immunofluorescence of B cells

For the immunofluorescence microscopy of BJAB and Raji D1.3 cells, fixed samples were prepared. Twelve-well PTFE diagnostic slides or microscope glass coverslips were coated with 4 µg/ml fibronectin for non-activated cells (45 minutes at 37°C). For activated cells, the slides were coated with 10 µg/ml of anti-human IgM $F(ab)_2$ or anti-mouse IgM $F(ab)_2$ as described in Chapter 3.3. Cells were seeded on twelve-well slides in the amount of approximately 30 000 cells per well in 30 µl of starvation medium (RPMI with 0.5% FCS), and 200 000 cells per well in 400 µl of the starvation medium on 10 mm glass microscope slides. Cells seeded on coated slides/coverslips were incubated at 37°C in 5% CO_2 for 15 minutes. Fixation was done by using 4% PFA and incubating the samples at room temperature for 20 minutes. Samples were then permeabilized using either 0.3% Triton-X in 1% BSA/PBS for 15 minutes or 0.5% Tween 20 in PBS for 10 minutes. Permeabilization was followed by blocking with 5% donkey serum for 10 minutes. After blocking samples were stained by incubating with primary antibodies for 45 minutes at room temperature, washing with PBS, and incubating with fluorophore-conjugated secondary antibodies for 45 minutes at room temperature. Samples were mounted with Fluoromont-G with DAPI.

3.4.2 Immunofluorescence of EVs

For immunofluorescence imaging of EVs fixed samples were prepared. Twelve-well PTFE diagnostic slides or microscope glass coverslips were coated with 10 µg/ml fibronectin, CellTak, or 0.01% Poly-L-Lysine. The volume of each coating solution was 30 µl for twelve-well slides and 400 µl for 10 mm glass coverslips. Fibronectin was incubated for 45 minutes at 37°C, CellTak was incubated for 45 minutes at RT, and Poly-L-Lysine was incubated for 10 min at RT on the shaker. Isolated EVs were then incubated on coated coverslips either by placing a drop of isolated EVs on parafilm and the coverslip on top or by putting the EVs on top of the coverslip and then placing the coverslip on the shaker. EVs were incubated on the coverslips for at least 1.5 hours. EVs were then fixed with 4% PFA incubated at RT for 20 minutes. Samples were then permeabilized using either 0.3% Triton-X in 1% BSA/PBS for 15 minutes. Permeabilization was followed by blocking with 5% donkey serum for 10 minutes. After blocking samples were stained by incubating with primary antibodies for 45 minutes at room temperature, washing with PBS, and incubating with fluorophore-conjugated secondary antibodies for 45 minutes at room temperature. Samples were mounted with Fluoromont-G.

3.5 EXPANSION MICROSCOPY SAMPLE PREPARATION

3.5.1 Method A

This method was used to expand B cells and EVs adhered to glass coverslips. First, immunofluorescence samples were prepared as described in Chapter 3.4, however, the samples were not mounted. After incubating the samples with primary and secondary antibodies the coverslips were washed with PBS and then submerged in Acryloyl-X (0.1 mg/ml) and incubated overnight at RT.

Gelation chambers [Figure 6] were prepared by wrapping microscope slides with parafilm and then attaching two 22 mm square coverslips to the parafilm by pipetting a drop of water between the glass and the parafilm. The distance between the coverslips was 6 mm.

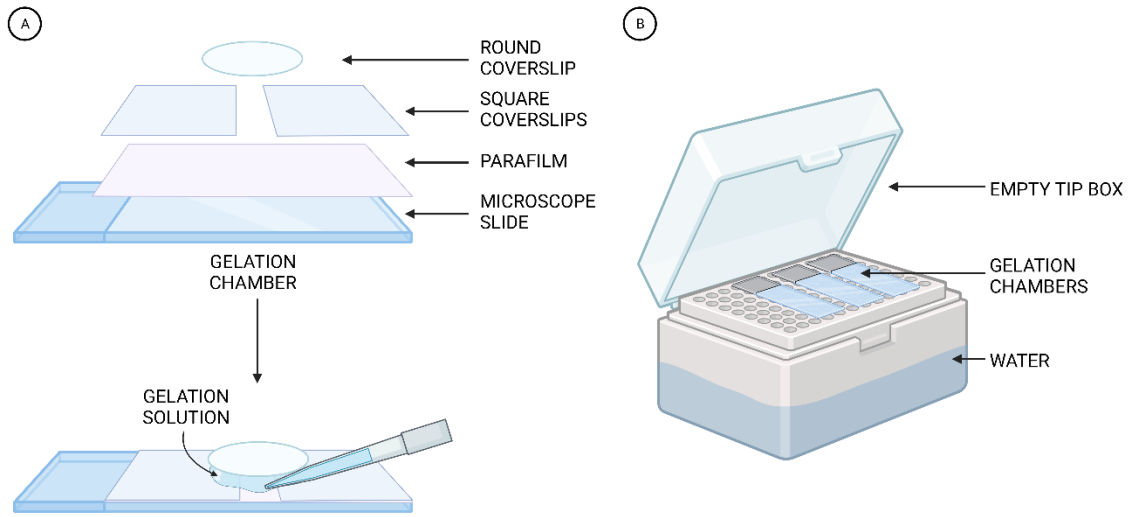

Figure 6 Schematic representation of gelation chambers. (A) Gelation chambers are used for the gelation step in expansion microscopy protocol. The gelation solution is pipetted on parafilm in the space between two square coverslips and the round coverslip is placed on top. If samples are prepared according to method A cells are seeded on the coverslip and the side containing the cells faces the gelation solution. **(B)** Gelation chambers are placed on the empty pipette tip box filled with water for the gelation time to provide humidity during the gelation.

The monomer solution (MS) was prepared by combining sodium acrylate (1.1 M), acrylamide (2.0 M), and MBAm (90 µg/ml) in PBS. MS was then aliquoted and stored at -20°C. Gelation solution (GS) was prepared by adding TEMED (1.5 mg/ml) and APS (1.5 mg/ml) to the monomer solution and vortexed for 5 sec. GS was kept on ice to prevent polymerization. Next, 60 µl of GS was pipetted into the gelation chamber [Figure 6]. The coverslip was then placed on top of the GS so that the side containing cells was facing the GS. The samples were then put in the empty pipette tip box filled with water to keep humidity and prevent the gels from drying and then incubated for 1h at 37°C [Figure 6]. After the incubation, the gelation chambers were kept for 15 min at RT to cool down. At

this point, the gelation solution polymerized forming a gel. Gels were then gently removed from the gelation chambers using a brush and placed in a 6-well plate in proteinase K solution (22.2 μg/ml in PBS) for digestion. Then the gels were washed four times in PBS for 30 minutes and stored in the fridge, in PBS overnight. The next day gels were incubated in the disruption buffer for 3h at 80°C. At this point, DAPI was added to the disruption buffer if necessary. After the incubation, the gels were rinsed with 0.4M NaCl and washed twice with PBS for 30 minutes. The gels were then transferred to Petri dishes and incubated in MQ water overnight. For imaging, small pieces of gel were cut and mounted on cell-imaging chambers.

3.5.2 Method B

This method was used to expand the EVs by putting them in the volume of the gel. First, isolated EVs were fixed by adding 4% PFA directly to the EVs in a 1:3 PFA to EVs ratio to obtain 1% PFA. EVs were then incubated with PFA for at least 1h or overnight. Then EVs were incubated with directly conjugated antibodies and membrane dyes for 1h at RT. This step was followed by adding Acryloyl-X (0.1 mg/ml) to the EVs and incubating them for more than 1h or overnight at RT.

Then, sodium acrylate (1.1 M), acrylamide (2.0 M), and MBAm (90 μg/ml) were added directly to the EVs, so that gel will be formed in the isolated EVs solution. This was followed by the addition of TEMED (1.5 mg/ml) and APS (1.5 mg/ml) to the monomer solution with EVs to create GS. The samples were then vortexed for 5 sec and kept on ice to prevent polymerization. Next, 60 μl of GS was pipetted into the gelation chamber [Figure 6] and the clean coverslip was placed on top of the gel to assure that the gel polymerizes in the right shape.

The next steps are the same as for method A. The samples were then put in the empty pipette tip box filled with water to keep humidity and prevent the gels from drying and then incubated for 1h at 37°C [Figure 6]. After the incubation, the gelation chambers were kept for 15 min at RT to cool down. At this point, the gelation solution polymerized forming a gel. Gels were then gently removed from the gelation chambers using a brush and placed in a 6-well plate in proteinase K solution (22.2 μg/ml in PBS) for digestion. Then the gels were washed four times in PBS for 30 minutes and stored in the fridge, in PBS overnight. The next day gels were incubated in the disruption buffer for 3h at 80°C. At this point, DAPI was added to the disruption buffer if necessary. After the incubation, the gels were rinsed with 0.4M NaCl and washed twice with PBS for 30 minutes. The

gels were then transferred to Petri dishes and incubated in MQ water overnight. For imaging, small pieces of gel were cut and mounted on cell-imaging chambers.

3.6 IMAGE ACQUISITION

Image acquisition was done using a spinning disc confocal microscope. Images were taken using 3i (Intelligent Imaging Innovations) Marianas spinning disc confocal microscope with 50 µm pinholes and Yokogawa CSU-W1 confocal scanner unit, and SlideBook 6 software. The objective used was a 63x Zeiss Plan-Apochromat oil immersion objective with NA = 1.4 and a working distance of 0.19 mm. Camera Hamamatsu sCMOS Orca Flash4.0 (2048 x 2048 pixels, 6.5x6.5 µm). The following lasers were used for sample imaging 405 nm (100mW), 488 nm (150mW), and 561 nm (100mW). Laser power was set to 30%. For z-stack imaging, the distance between the optical slices was set to 300 nm.

3.7 WESTERN BLOTTING

Western blots of isolated EVs and whole cell lysates for activated and non-activated BJAB and Raji D1.3 cell lines were done using 4–15% precast polyacrylamide gels in non-reducing conditions. Whole-cell lysates were sonicated to facilitate loading them into the gel. The protein concentration of each sample was measured using a BCA assay. Samples were first boiled for 5 minutes at 95°C with 4xSDS Laemmli sample buffer. Equal amounts of protein were then loaded into the gel and the western blot was run at 40 mA in Laemmli buffer. Proteins were then transferred to nitrocellulose using Trans-Blot Turbo Mini 0.2 µm Nitrocellulose Transfer Packs. Membranes were blocked in 5% milk in TBS-t for 30 minutes and incubated at +4°C in primary antibodies overnight. Then the membranes were washed in TBS-t, incubated in HRP-linked secondary antibodies, and washed again in TBS-t. HRP substrate was added before imaging and the images were acquired using BioRad ChemiDoc MP Gel Analyzer.

3.8 SIZE EXCLUSION CHROMATOGRAPHY (SEC)

SEC was done using Izon qEV1 columns. At least 60 000 000 cells per cell line were collected. The cells were then centrifuged at 1300 rpm for 2 minutes and then resuspended in 2 ml of starvation RPMI containing 0.5% exosome-free FCS medium. This step was repeated twice to get rid of cell culture medium components. Then 2 ml of cell suspension was divided into two tubes so that 1 ml of cells was then activated using soluble activation as described in Chapter 3.3, and the remaining 1 ml was not activated. Both activated and

non-activated cells were then incubated for 30 minutes at 37°C. To collect the EVs-containing medium the cells were centrifuged at 1500g for 10 minutes at 4°C. This removed cells and large cellular debris from the supernatant. The supernatant was then collected and re-centrifuged at 10 000g for 10 minutes at 4°C [Figure 7]. After centrifugation supernatant containing EVs was kept on ice. The remaining cells pellet was lysed with Triton-X Lysis Buffer.

Prior to SEC Izon qEV1 columns were flushed with 13.5 ml of filtered PBS. 1 ml of EV-containing supernatant was then loaded into the columns followed by 13.5 ml of filtered PBS. The first 4 ml of the eluate was discarded as it does not contain EVs. The remaining 10 ml of eluent was collected and kept on ice.

3.9 EV CONCENTRATION

After EV isolation using SEC (Chapter 3.8), the samples were concentrated using Amicon Ultra-15 Centrifugal Filter Units. Around 10 ml of EV-containing SEC eluent was loaded into concentration tubes. The samples were then centrifuged at 3180g for 20 minutes at 4°C using a swing bucket rotor. The samples were then collected and stored on ice or at 4°C. The average volume of isolated EVs after concentration was around 200 µl.

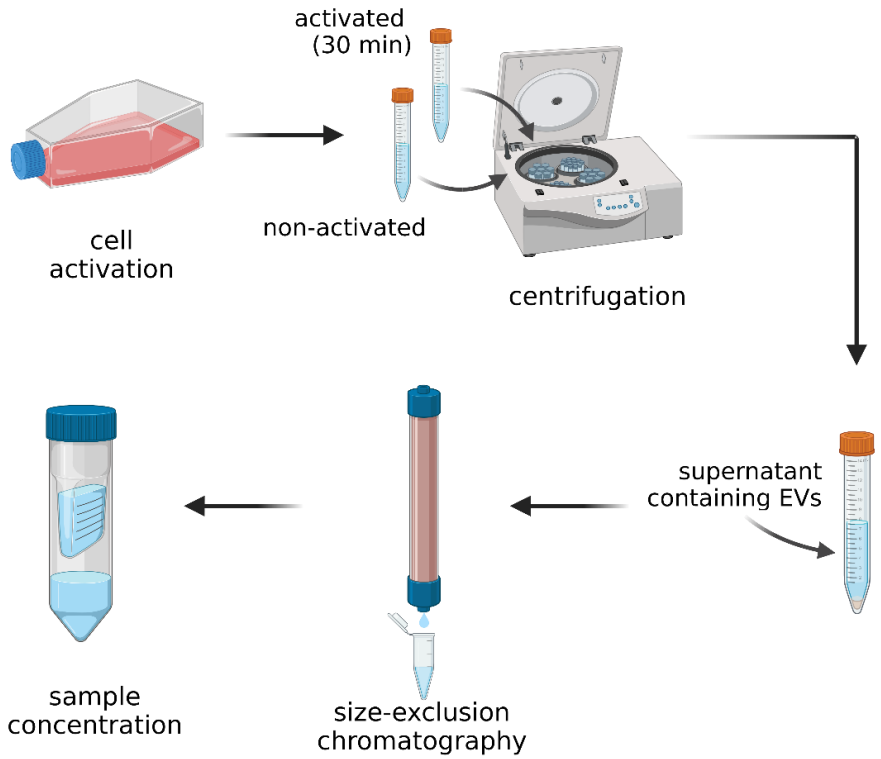

Figure 7 Schematic diagram of EVs isolation. Activated and non-activated cells were incubated for 30 minutes. Then the samples were centrifuged and the supernatant containing EVs was collected. EVs were then isolated from the supernatant using size-exclusion chromatography (SEC). Isolated EVs were then concentrated using concentration tubes

3.10 Image processing and analysis

Cell and nuclei segmentation and MFI measurements were done using CellProfiler 4.2.4. The perinuclear area was determined based on the DAPI channel and the cell area was determined on the membrane/phalloidin channel. To obtain the cytoplasm area nuclei mask was subtracted from the cell mask. MFI was measured from the tetraspanin CD63 or CD81 channel using perinuclear and cytoplasm masks as ROI. The ratio between the MFI of tetraspanins measured in the perinuclear area and the cytoplasmic area was calculated for each cell.

3.11 Statistical analysis and illustrations

Statistical significance was calculated paired Student's t-test, assuming a normal distribution of the data. P values were indicated as follows: * $P \leqslant 0.05$, ** $P \leqslant 0.01$, *** $P \leqslant 0.001$. Graphs and statistical analysis were done using GraphPad Prism 8. Illustrations were created using BioRender. 3D visualization of the cell was done using ImageJ 3D Viewer plugin and processed in Blender 2.93.

4 RESULTS

4.1 ANALYSIS OF CHANGES IN INTRACELLULAR LOCALIZATION OF CD63 AND CD81 UPON B CELL ACTIVATION

Tetraspanins CD63 and CD81 are associated with intracellular vesicle trafficking and EV secretion. B cell activation can lead to alterations in vesicular trafficking and increased EV secretion. Here, the alteration in intracellular localization of CD63 and CD81 upon B cell activation was examined. The study focused on the comparison between tetraspanin localization in the perinuclear area and the rest of the cell, here referred to as cytoplasm. Preliminary imaging data suggested that CD81 might move from the cellular membrane toward the nucleus upon activation while CD63 seemed to cluster in the perinuclear area in non-activated B cells and appeared to move toward the plasma membrane upon B cell activation. To confirm these observations three independent experiments were conducted to study CD81 and CD63 localization. Each experiment was conducted on both Raji D1.3 and BJAB cell lines.

To induce cell activation, B cells were plated on anti-IgM while non-activated cells were plated on fibronectin (see Chapter 3.3). Cell activation was assessed by pBtk signaling or visually by cell spreading. Z-stack images were acquired using a spinning disc confocal microscope. For an automated cell segmentation and analysis the middle slices of the z-stack were chosen as they represent approximately the middle of the cell in the z-direction [Figure 8]. This choice was based on the observation, that the middle plane displayed a representative distribution of tetraspanins in the cells and allowed for clear visualization of alterations in its localization.

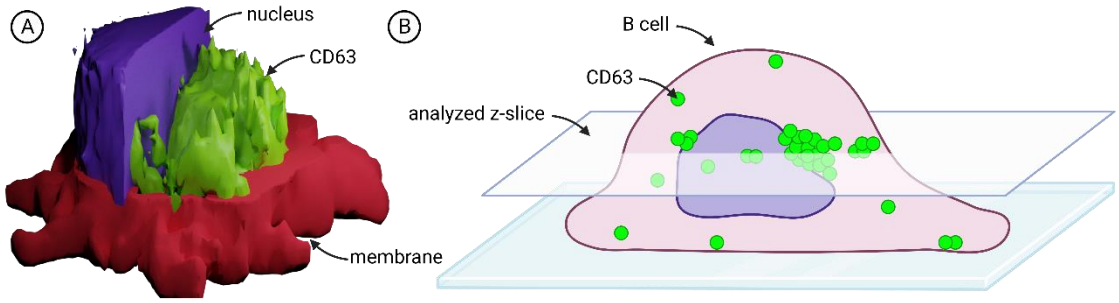

Figure 8 Schematic representation of CD63 distribution in B cells. The CD63-positive vesicles were predominantly located in the central region along the z-axis of the cell. **(A)** 3D render of non-activated BJAB cell with selective removal of membrane and nucleus sections to improve visualization of CD63 distribution. **(B)** A schematic diagram illustrating the selected z-slice for image analysis. The middle z-slice of the image stack was selected as representative of changes in CD63 localization upon B cell activation. For this reason, further quantification was done on the slice marked here as an *analyzed z-slice.*

The mean fluorescence intensity (MFI) of each tetraspanin was measured both in the perinuclear area and the cytoplasm [Figure 9]. The MFI ratios of the perinuclear area to cytoplasm were calculated for each activated and non-activated cell. Calculated ratios were then compared between activated and non-activated cells.

The comparison of the CD63 MFI ratio between activated and non-activated cells showed a statistically significant difference only for Raji D1.3 cells [Figure 10]. In this cell line, $MFI_{perinucleus}/MFI_{cytoplasm}$ ratio indicated a higher MFI of CD63 in the perinuclear area than in the cytoplasm area in activated cells. This suggests that the activated Raji D1.3 cells showed translocation of CD63 towards the perinuclear area, while in BJAB cells localization of CD63 remained the same. It is not clear whether the inconsistency of the results is due to the differences in sample size or high variability in the measurements, or is caused by phenotype differences between the cell lines. For the above reasons, more data should be acquired to confirm the results, including different B cell lymphoma cell lines. Alternatively, different analysis methods may need to be employed to determine if other factors are affecting the results.

The comparison of the CD81 MFI ratio between activated and non-activated cells didn't show a statistically significant difference either in BJAB or in Raji D1.3 cells [Figure 11].

The translocation of CD63 and CD81 between the perinuclear area and the cytoplasm upon B cell activation could indicate their involvement in intracellular signaling pathways and antigen presentation, as well as the formation and release of extracellular vesicles. Their translocation would suggest that they might play an important role in B cell activation and provide insights into the regulation of B cell functions and potential therapeutic targets.

The results obtained from the experiments, done using conventional spinning-disc confocal microscopy, do not provide a strong answer on whether or not B cell activation affects the intracellular localization of tetraspanins, especially CD63. Further analysis, including different z-positions and 3D volume MFI measurements, could be conducted to investigate tetraspanin expression in activated B cells. The technical difficulty of analyzing the perinuclear area may have influenced the obtained results. In some cells, the movement of tetraspanins toward the nucleus did not result in localization in the nuclear grooves within the segmented nuclei area, but instead in the perinuclear region. Defining this area for image analysis can be challenging and requires determining a region at a specific distance from the nucleus, as it cannot be directly segmented from actin or

membrane staining. Developing an image analysis approach that can detect more subtle changes in localization may be beneficial for future studies.

Another issue in imaging tetraspanin-positive vesicular structures is that many of the vesicles fall under the resolution limit of light microscopes therefore they might not have been well resolved in the acquired images. To overcome this issue expansion microscopy (ExM) was used as a tool allowing to increase the resolution by physically expanding the sample without the need of using specialized super-resolution equipment.

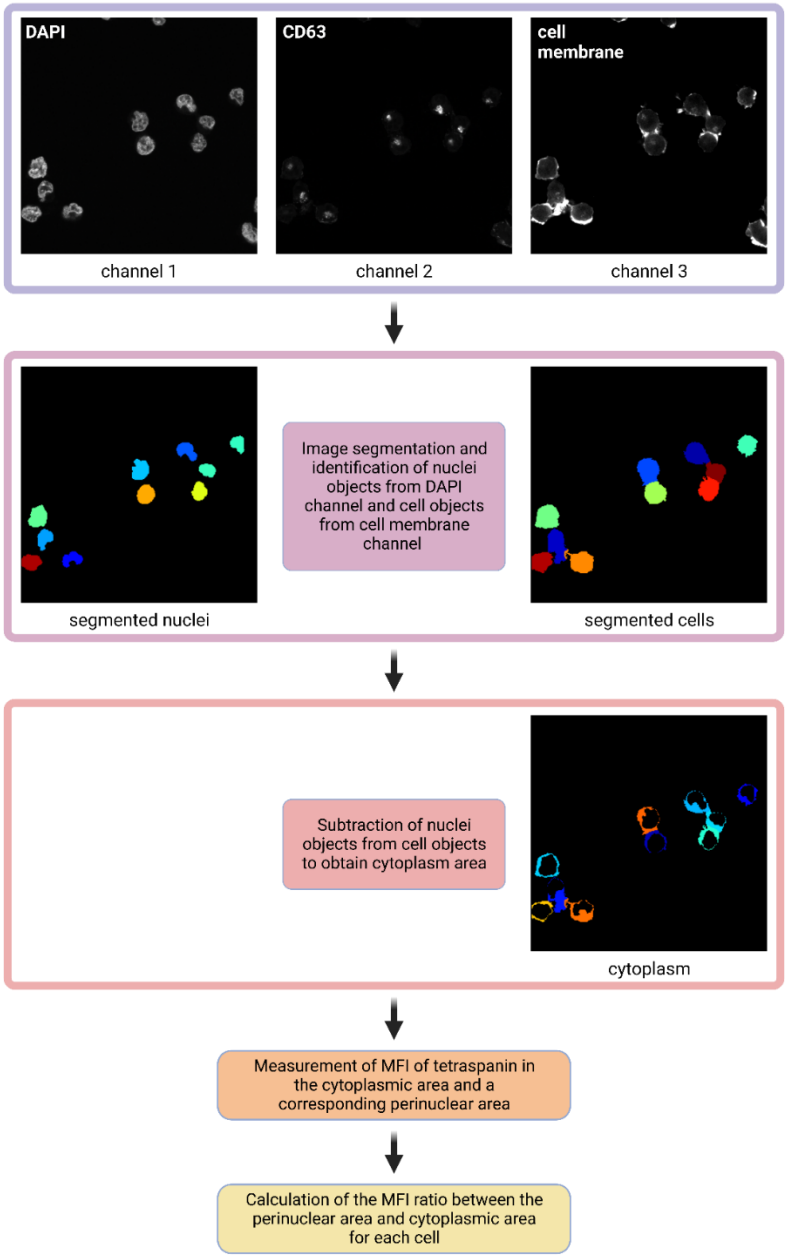

Figure 9 Image segmentation and MFI measurement workflow. Cells were segmented based on the DAPI channel and cell membrane/actin channel. From the DAPI channel nuclei, objects were obtained and from the cell membrane/actin channel, cell objects were obtained. The nuclei were then subtracted from cells in order to obtain cytoplasm area objects. The next step was the measurement of the MFI of tetraspanins CD63 and CD81 in the cytoplasmic area and corresponding perinuclear area. In the end, a ratio between the MFI of tetraspanins in the perinucleus and the MFI of the tetraspanins in the cytoplasm was calculated for each cell. Cells partially located beyond the edge of the image were not analyzed.

CD63 translocation

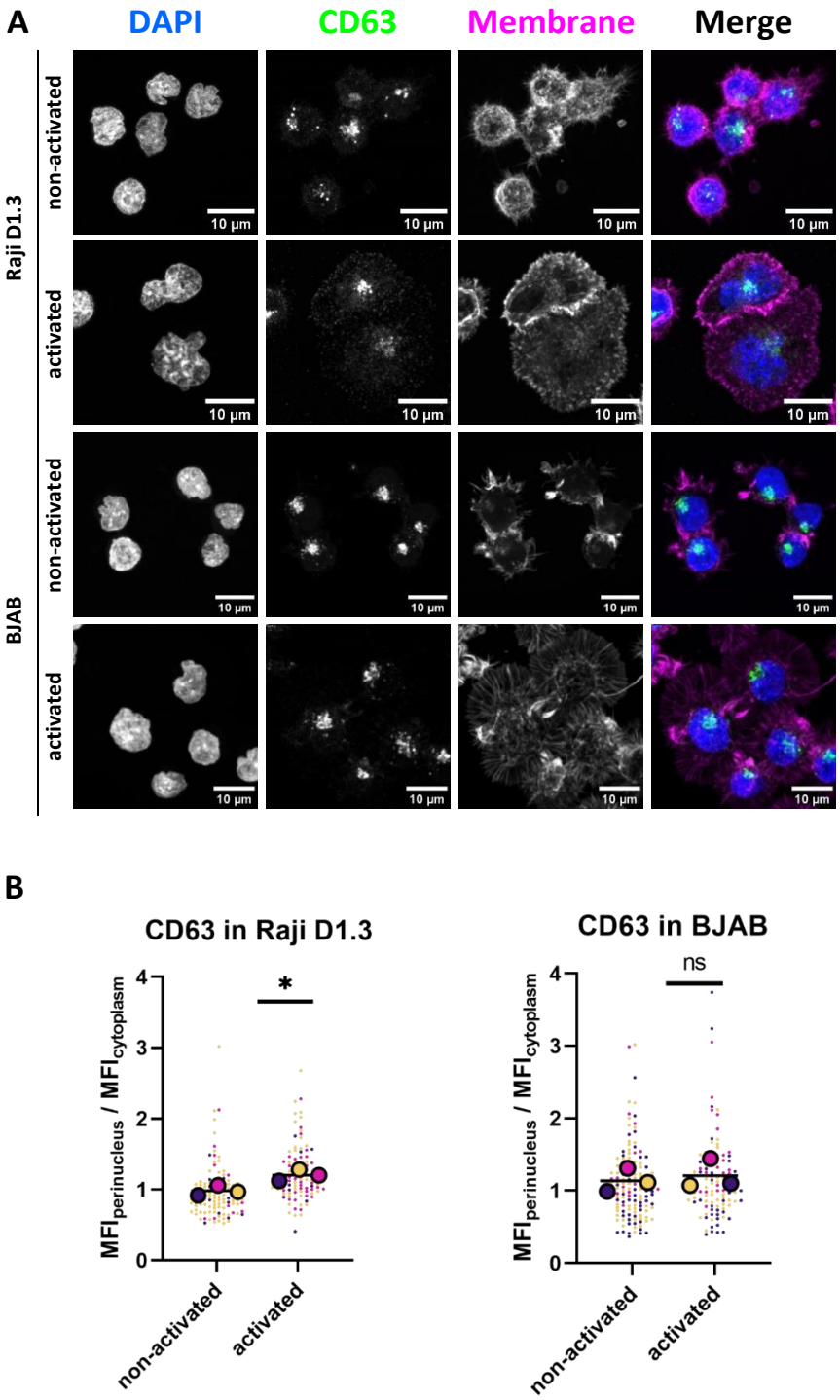

Figure 10 CD63 translocation analysis. The aim was to investigate if CD63 translocates from the perinuclear area of non-activated B cells to the cytoplasm upon activation. **(A)** Imaging of non-activated and activated (membrane-bound activation, 15 min) Raji D1.3 and BJAB cells using a spinning disc confocal microscope. Cells were fixed, labeled with anti-CD63 antibody, and stained with DAPI and MemGlow (membrane). Maximum intensity projection images of representative cells are shown. **(B)** Mean fluorescence intensity (MFI) analysis of CD63 expression in the perinuclear area and cytoplasm of activated and non-activated Raji D1.3 and BJAB cells. Middle slices of the z-stack were analyzed as they displayed a representative distribution of tetraspanins. Higher $MFI_{perinucleus}/MFI_{cytoplasm}$ ratio values indicate that more CD63 was present in the perinuclear area of the cell than in the cytoplasm. Results show that CD63 translocates to the perinuclear area in activated Raji D1.3 cells. The number of cells analyzed in each experiment equals 18,48, and 72 for experiments 1, 2, and 3, respectively in non-activated BJAB cells, 24,36, and 41 in activated BJAB cells, 12,13, and 86 in non-activated Raji D1.3 and 38,10, and 44 in activated Raji D1.3. Each independent experiment is represented by a different color. Small symbols represent individual cells and large symbols represent the mean of each experiment. The mean of all three experiments is represented with a line. * $P \leqslant 0.05$, ns – non-significant, paired t-test (n=3).

CD81 translocation

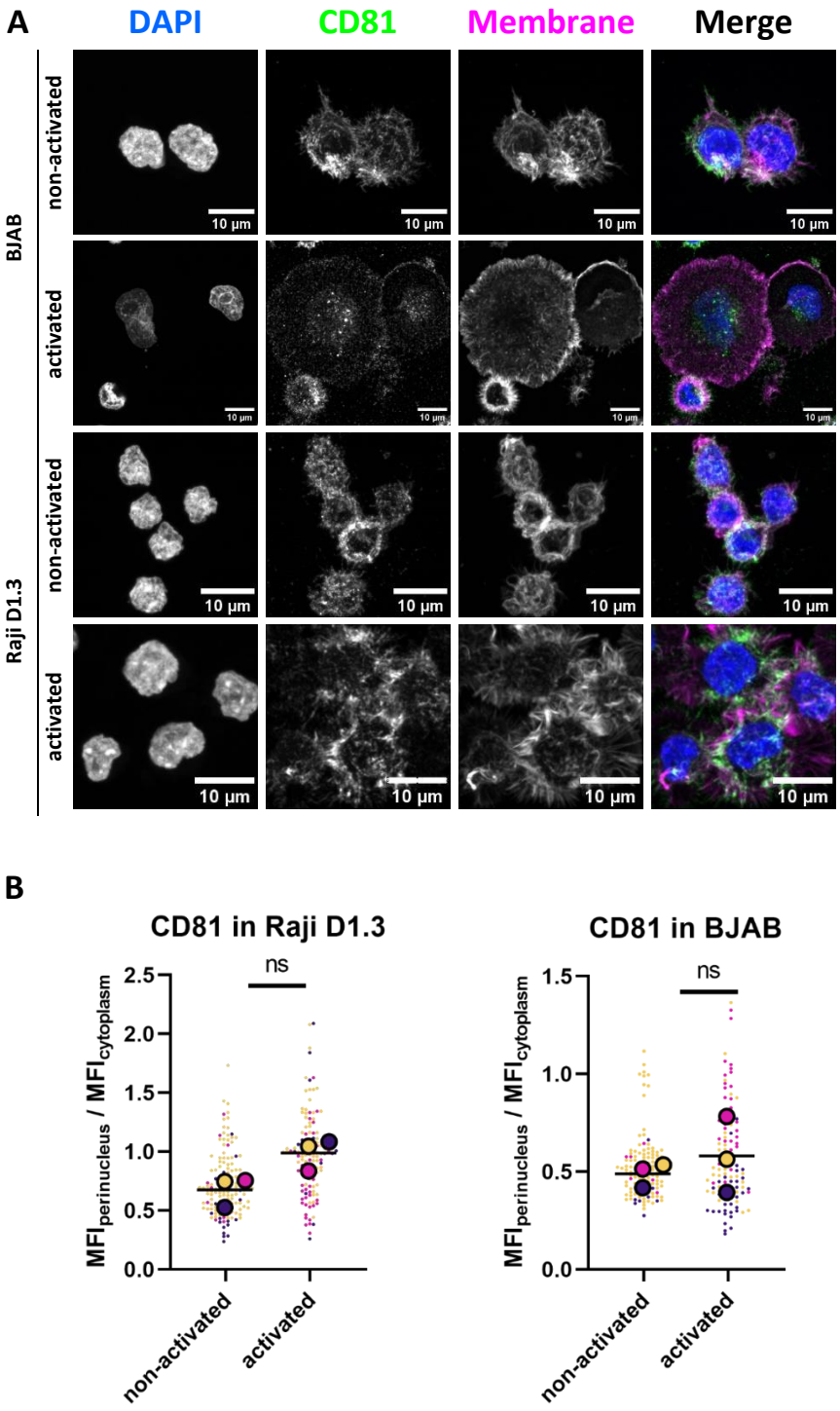

Figure 11 CD81 translocation analysis. The aim was to investigate if CD81 translocates from the cytoplasm of non-activated B cells to the perinuclear area upon B cell activation. **(A)** Imaging of non-activated and activated (membrane-bound activation, 15 min) Raji D1.3 and BJAB cells using a spinning disc confocal microscope. Maximum intensity projection images of representative cells are shown. **(B)** Mean fluorescence intensity (MFI) analysis of CD81 expression in the perinuclear area and cytoplasm of activated and non-activated Raji D1.3 and BJAB cells Middle slices of the z-stack were analyzed as they displayed a representative distribution of tetraspanins. Higher $MFI_{perinucleus}/MFI_{cytoplasm}$ ratio values indicate that more CD81 was present in the perinuclear area of the cell than in the cytoplasm. No translocation of CD81 upon B cell activation was observed. The number of cells analyzed in each experiment equals 10,13, and 107 for experiments 1, 2, and 3, respectively in non-activated BJAB cells, 31,34, and 41 in activated BJAB cells, 11,10, and 112 in non-activated Raji D1.3 and 48,12, and 71 in activated Raji D1.3. Each independent experiment is represented by a different color. Small symbols represent individual cells and large symbols represent the mean of each experiment. The mean of all three experiments is represented with a line. ns – non-significant, paired t-test (n=3)

4.2 High-resolution imaging of B cells using Expansion Microscopy

In images acquired using fluorescence microscopy identifying small structures such as vesicles can be challenging due to their tendency to appear clumped together. ExM is an alternative tool that provides super-resolution images without the need for a specialized super-resolution microscope. Here, ExM was used to visualize the distribution of CD63 in Raji D1.3 cells. The protein retention ExM protocol [73] was optimized to be used with

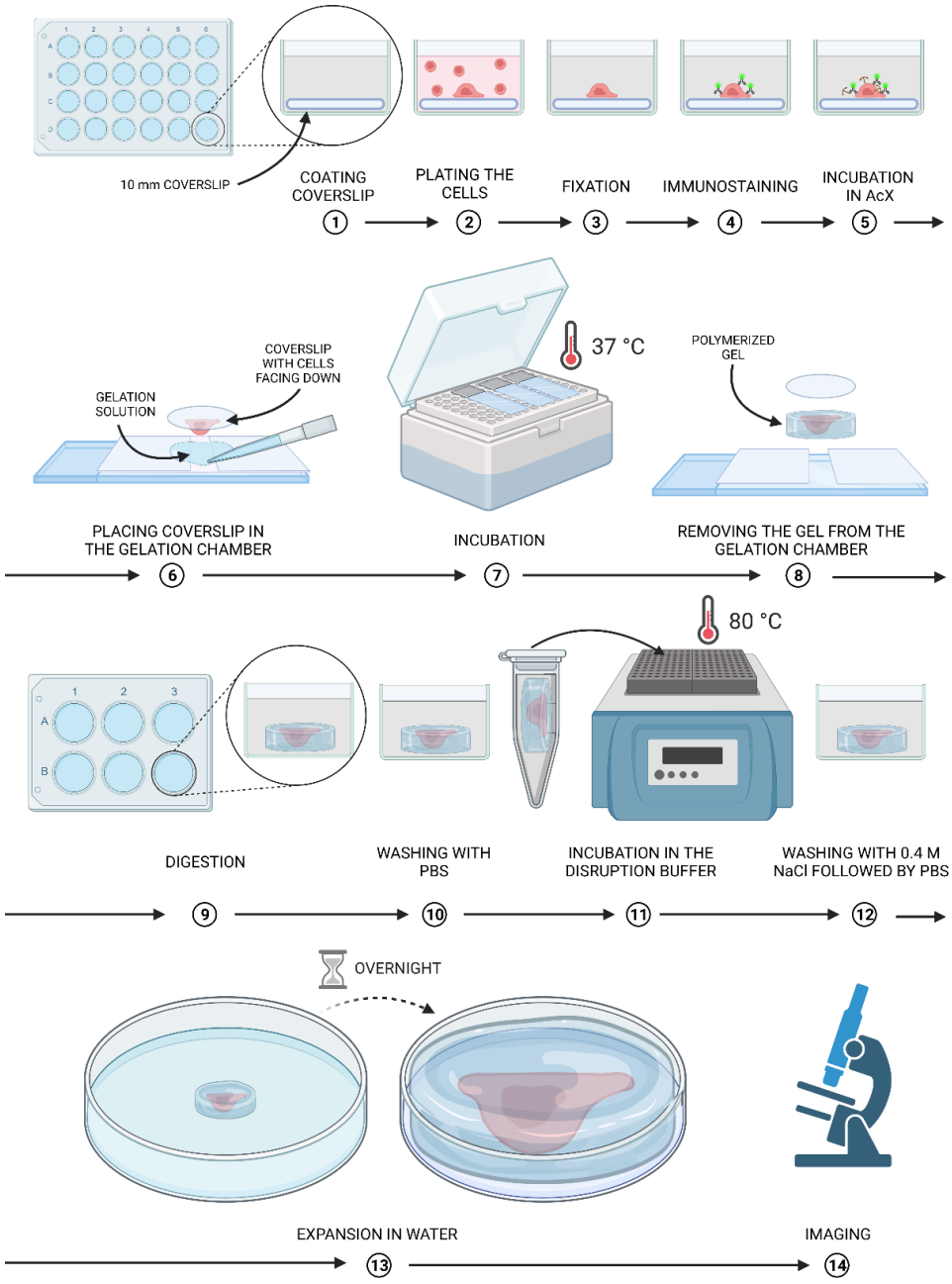

Figure 12 Expansion microscopy workflow. Steps 1-4 are typical immunostaining steps, where molecules of interest are labeled with fluorescent probes. In step 5 sample is incubated overnight in AcX to enable protein anchoring in the gel by modifying amines present in the proteins. In steps, 6-8 gel is formed from the gelation solution by polymerization of the solution components together with the sample. Steps 9-12 aim to homogenize the mechanical properties of the gel and enable uniform expansion by proteolytic digestion of the gel meshwork. In step 13 sample is expanded in MQ water overnight. Expansion is a result of gel swelling driven by the osmotic force that drives water diffusion into the gel. Step 14 is sample imaging using a confocal microscope.

B cells [Figure 12]. The expansion factor of the gels was estimated based on the size of the gel before and after expansion, and, depending on the experiment, it amounted to approximately five-fold to ten-fold expansion. Differences in the expansion factor could be a result of slight variations in the gel preparation or differences in incubation time.

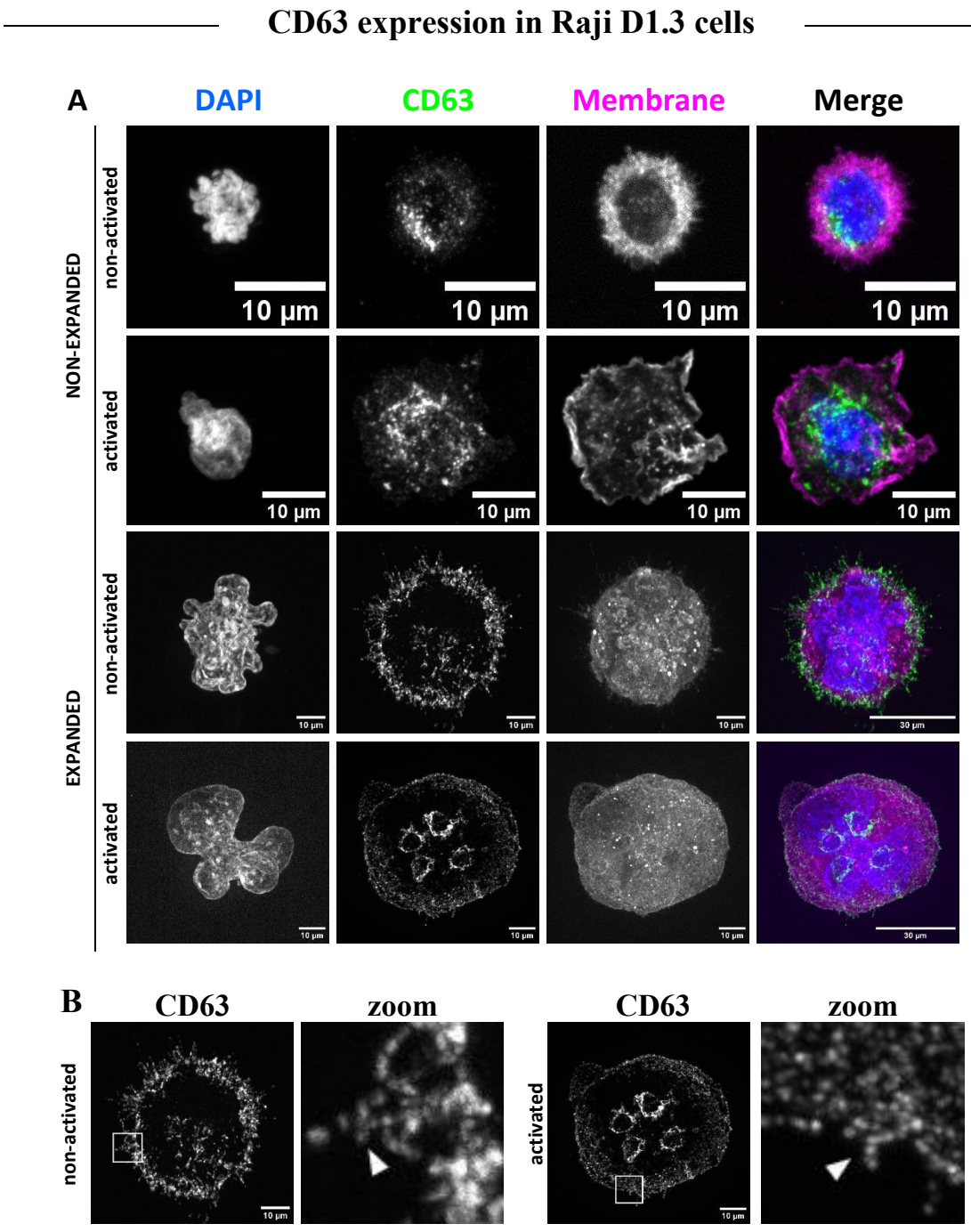

Figure 13 Comparison of CD63 expression in Raji D1.3 cells using standard immunofluorescence and expansion microscopy. (A) Cells are shown using maximum-intensity projection images, with the scale bar of the expanded cells representing the size of the cell after expansion, not its actual size. The cell phenotype characterized by the expression of CD63 on the cell membrane rather than the nucleus that can be seen in a non-activated expanded cell was noted across multiple ExM images. This goes in line with the image analysis performed on IF images in Chapter 4.1. MemGlow dye was used for membrane staining for IF images and MembraneExM for ExM images. **(B)** The arrowhead indicates round CD63 points. Maximum intensity projection images are shown, with white squares highlighting a region of interest that was zoomed in to provide better visualization of CD63 distribution.

Table 3 Summary of Raji D1.3 cells imaged using expansion microscopy. The table shows data from all the cells that were imaged. For both non-activated and activated samples, the number of cells where the CD63 was located predominantly in the perinucleus and the cytoplasm is shown. The table shows data from three independent experiments. The assessment of CD63 intracellular localization was done through a visual examination of images, with no measurement taken. Thus, the resulting observations are subjective and insufficient to conclude alterations in CD63 intracellular localization. However, it is worth noticing that in all imaged non-activated cells CD63 was observed to localize predominantly in the cytoplasm, and in the majority of imaged activated cells CD63 localized predominantly in the perinuclear area, which is in agreement with the quantification of CD63 localization presented in Chapter 4.1.

	Non-activated		**Activated**	
	Cell count with CD63 primarily in perinucleus	Cell count with CD63 primarily in the cytoplasm	Cell count with CD63 primarily in perinucleus	Cell count with CD63 primarily in the cytoplasm
Experiment 1	-	-	7	2
Experiment 2	-	7	6	5
Experiment 3	-	-	2	-

ExM proved to be a useful technique in this study as it allowed for the identification of the distribution pattern of CD63 in Raji D1.3 cells with high precision and resolution higher than with a standard confocal microscope [Figure 13]. Vesicular structures are shown more clearly and smaller structures can be distinguished in what appeared to be a vesicular clump in standard IF images. Although expanded images allow us to more precisely estimate the location of vesicles in the cell, both sample preparation and imaging are all more laborious and time-consuming therefore less suitable for obtaining a high number of cells that would be suitable for quantification. Even though three experiments were conducted, the number of images possible to acquire wasn't big enough to give a representative overview of cell populations imaged with ExM. A significant issue encountered during image acquisition was hydrogel drift. Post-expansion hydrogel drift is a known issue in ExM microscopy [86]–[88], however, it was not always possible to prevent it, which significantly limited the number of imaged cells and acquired z-stacks. For this reason, ExM images could not be quantified using a similar workflow as the one described in Chapter 4.1. However, after visual assessment of acquired images it can be noticed that in all the non-activated Raji D1.3 cells imaged using ExM, CD63 was located predominantly in the cytoplasm, while in the majority of activated cells, CD63 was located predominantly in the perinuclear area [Table 3]. This supports the results obtained by the analysis of IF images of Raji D1.3 cells in Chapter 4.1, where CD63 was shown to localize in the perinuclear area upon B cell activation.

4.2.1 Selection and implementation of the permeabilization method

To be able to visualize membranous and actin structures with expansion microscopy, Chrometra ActinExM, and MembraneExM probes were used. Those probes can be copolymerized with the gel as opposed to typically used fluorophores that target small molecules, such as phalloidin. Some of the standard IF probes have been shown to be incompatible with ExM due to the difficulty to link them with the gel matrix and washing them out of the sample during the ExM sample preparation process [86]. Before preparing ExM samples, ActinExM and MembraneExM staining were optimized with both BJAB and Raji D1.3 cell lines using standard IF on a spinning disc confocal microscope. Optimized dilutions of the fluorophores were then used for ExM sample preparation.

ActinExM is added to the sample following immunostaining and incubation with AcX. As ActinExM does not require a specialized sample preparation protocol, samples were first prepared according to the standard protocol of PFA fixation, permeabilization in 0.3% Triton-X in 1% BSA/PBS followed by blocking. However, the manufacturer of MembraneExM recommended using permeabilization with 0.5% Tween 20 instead of 0.3% Triton-X, which led to the question of which permeabilization method is most appropriate for visualizing CD63 and CD81 in B cells. To investigate the difference, both permeabilization methods were tested with MembraneExM and ActinExM probes [Figure 14]. The sample preparation steps for both Triton-X and Tween 20 permeabilized samples were identical in this experiment. The images were acquired using the same acquisition settings, which leads to the conclusion that any differences observed are solely due to the selected permeabilization method.

A strong difference was observed in the MembraneExM signal intensity between 0.5% Tween 20 and 0.3% TritonX permeabilization methods. 0.5% Tween 20 permeabilization resulted in images that were oversaturated, requiring the use of lower concentrations for subsequent experiments. Conversely, no notable difference was observed in the ActinExM samples, which showed a good signal with both methods. 0.5% Tween 20 permeabilization yielded high-quality staining of CD81 and CD63. Although tetraspanin staining appeared similar between the two permeabilization methods, 0.5% Tween 20 seemed to better preserve tetraspanin-positive membrane protrusions [Figure 14].

Approximately 100 cells were analyzed in this comparison, and based on the results, 0.5% Tween 20 permeabilization was selected for further experiments. The images presented in Chapter 4.2 were acquired using 0.5% Tween 20 permeabilization.

Comparison of permeabilization methods

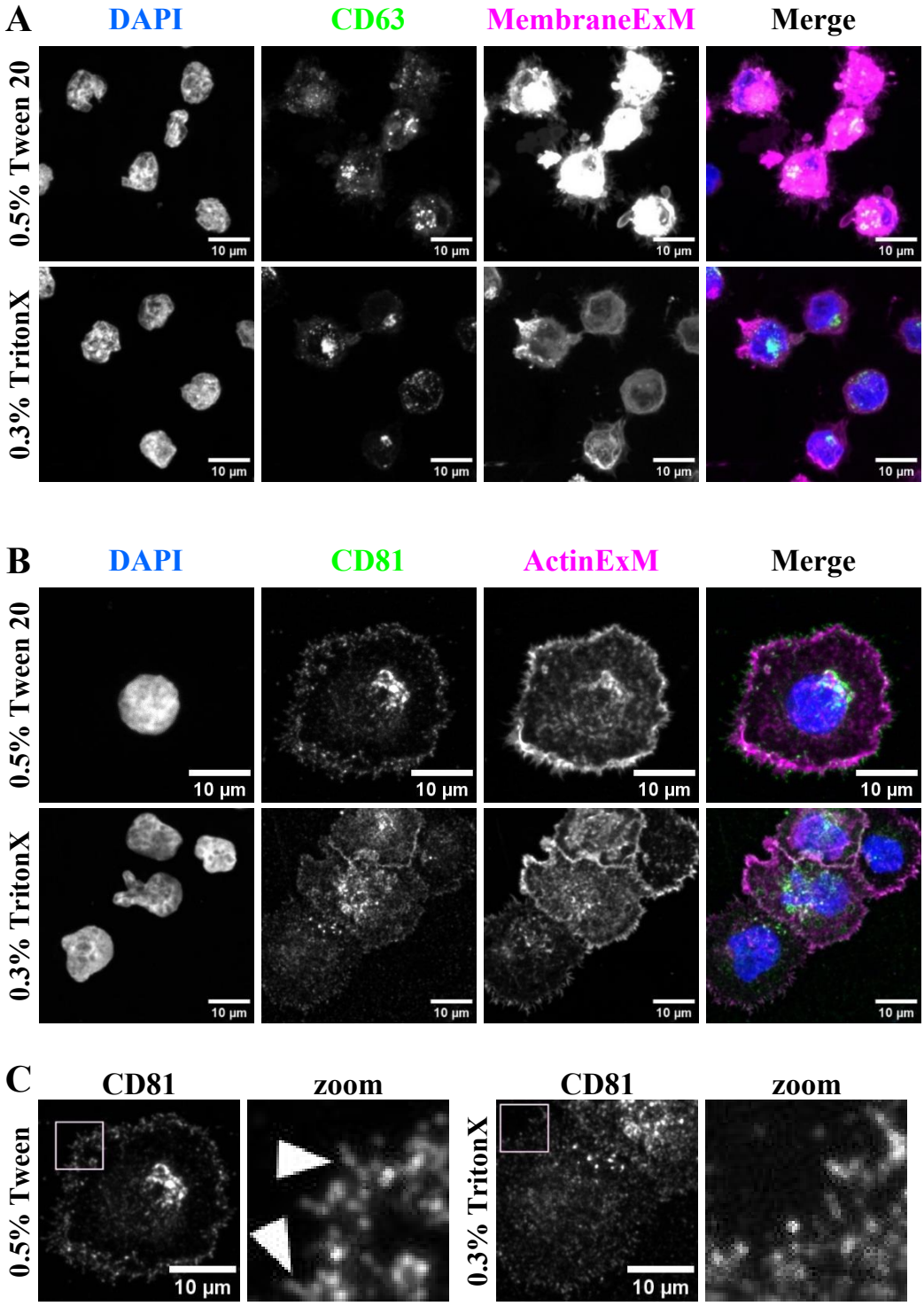

Figure 14 Comparison between different permeabilization methods. IF images were acquired using a spinning disc confocal microscope. Representative cells are shown using maximum-intensity projection images. **(A)** MembraneExM dye gives a significantly brighter signal with 0.5% Tween permeabilization as compared to 0.3% Triton-X. Images show non-activated Raji D1.3 cells. **(B)** The intensity of the ActinExM signal remains similar regardless of the permeabilization method. Images show activated Raji D1.3 cells. **(C)** Comparison of CD81 staining with different permeabilization methods. The arrowhead indicates examples of membrane protrusions that were preserved with 0.5% Tween 20 permeabilization. Maximum intensity projection of CD81 staining of representative cells is shown. In CD81 images, the white square highlights a region of interest that was zoomed in to provide a better overview of structures preserved with different permeabilization methods.

4.3 VISUALIZING EVS USING EXPANSION MICROSCOPY

Recent advances in super-resolution imaging have enabled researchers to expand their understanding of the structure and functioning of EVs. Given the small size range of EVs, super-resolution techniques play a critical role in enabling their imaging. Conventional confocal microscopy is typically inadequate for imaging EVs due to their small size, particularly for the smaller vesicles that fall below the resolution limit of light microscopes. However, ExM differs from other super-resolution techniques as it allows for high-resolution images to be obtained using standard confocal microscopes. This technique holds great potential for advancing our understanding of EVs and their roles in various biological processes. To the best of our knowledge, ExM has never been used for imaging EVs, hence this study aimed to develop a method of imaging EVs using ExM.

4.3.1 Western blot analysis of SEC-isolated EVs

EVs were isolated from activated and non-activated BJAB and Raji D1.3 cells using SEC [Figure 15]. The presence of EVs in the isolated samples was assessed using Western Blott (WB). The presence of selected proteins in EVs and whole cell lysates (WCL) of the cells from which the EVs were isolated was evaluated using WB for activated and non-activated cells from Raji D1.3 and BJAB cell lines. Equal amounts of protein were loaded onto the gel as measured with the BCA assay. GAPDH was used as a loading control. Ezrin, Cathepsin S, and CD81 were used as vesicular markers and pBtk was used as a B cell activation marker. WB was repeated 2-4 times with similar results [Figure 15].

The results of the Western blot analysis indicate the presence of isolated EVs in the samples. Ezrin showed significantly higher expression levels in both activated and non-activated EVs in both cell lines, as compared to the WCL. Ezrin is a protein that is associated with cellular membranes and exocytosis, therefore increased ezrin signal intensity in the samples indicates the presence of EVs in the isolated material.

In contrast, cathepsin S displayed differential expression patterns in the two cell lines. Specifically, Raji D1.3 cell line, cathepsin S expression was relatively consistent in both EVs and WCL. In BJAB cells, however, the signal was stronger in the WCL of both activated and non-activated cells. Cathepsin S can be secreted in lysosomal or endosomal vesicles, therefore its presence in the isolated sample indicates the vesicular nature of the studied material. Differences in cathepsin S expression between the cell lines might reflect possible differences in vesicular landscape between them, however, the presence of cathepsin S in each of the isolated EV samples indicates EV presence.

Western blot of SEC-isolated EVs

A

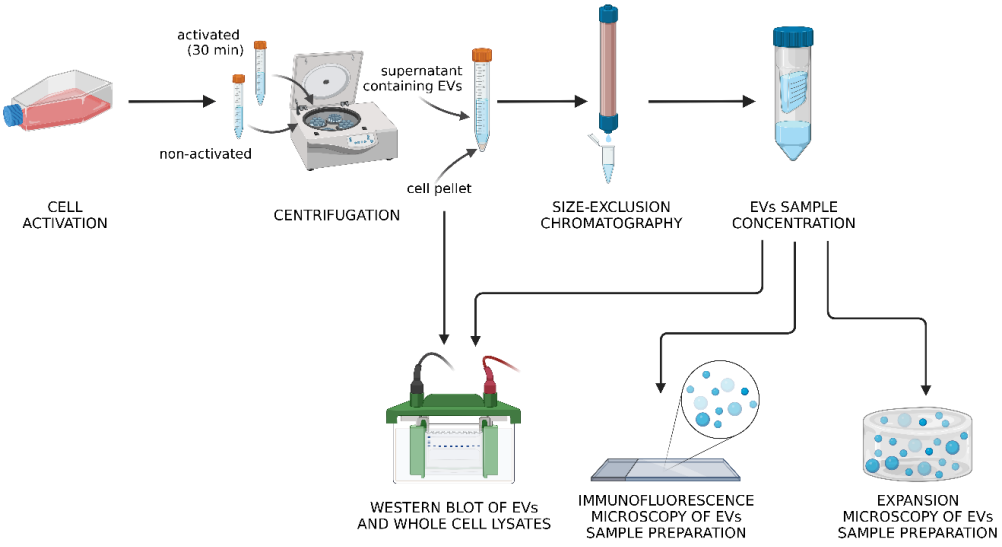

B

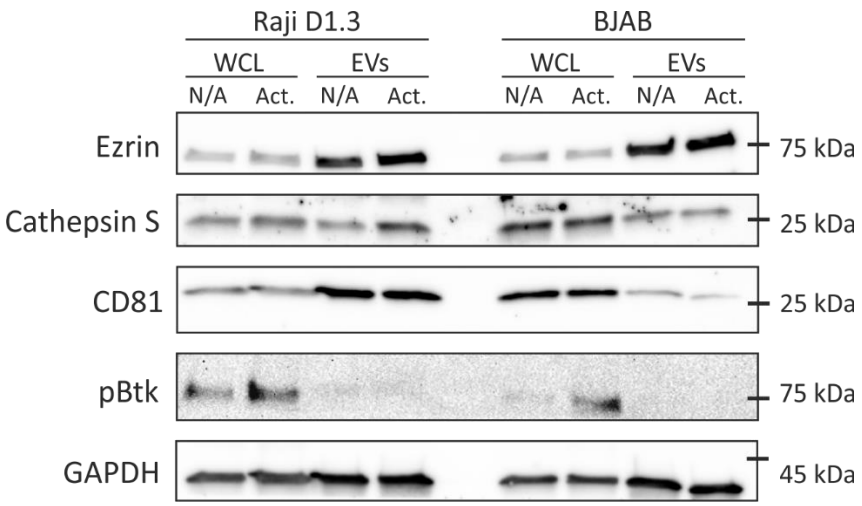

Figure 15 Western blot of SEC isolated EVs and whole cell lysates (WCL). (A) Schematic workflow of EVs isolation. Cell pellet obtained after sample centrifugation was lysed and then used for the Western blot analysis. Size exclusion chromatography was then carried out on the sample, followed by sample concentrations. Isolated EVs were then used to prepare ExM samples, IF samples, and Western blot analysis. **(B)** Western blot analysis. EV markers are detectable in the samples by Western blot analysis. Equal amounts of WCL and corresponding EV samples were analyzed for the expression of Ezrin, Cathepsin S, and CD81. GAPDH was used as a loading control and pBtk as a B cell activation marker. N/A – non-activated. Act. – Activated.

CD81 is a commonly used EV marker, however, its presence is not exclusive to EVs. Here, CD81 exhibited more intense expression levels in EVs of Raji D1.3 cells and the WCL of BJAB cells. Despite the more intense signal intensity in BJAB WCL, the presence of CD81 in EV samples indicates the presence of EVs.

pBtk is a marker of B cell activation and was used to confirm the successful activation of the cells. WB demonstrated the strongest pBtk signal in activated cells indicating that the

B cells were indeed activated. The residual pBtk signaling in non-activated Raji D1.3 cells might be a result of basal BCR signaling that is present in non-activated B cells.

GAPDH was used as a loading control for the WB analysis and expressed relatively constant levels across all the samples tested, suggesting equal protein loading and ensuring that the experiments accurately reflected differences in protein expression levels between the samples

4.3.2 Sample preparation optimization for immunofluorescence imaging of EVs

As ExM protocol requires the preparation of standard IF samples prior to the gelation process, it was first necessary to image EVs using a standard confocal microscope. This section describes a sample preparation for the immunofluorescence imaging of EVs.

Before performing ExM, EVs needed to be attached to the coverslips, fixed, and stained as normal IF samples. Three different slide coatings were tested for both activated and non-activated EVs using confocal microscopy in order to choose the one that gives the best results. We compared fibronectin, CellTak, and Poly-L-Lysine. The results, as evaluated by the number of EVs found as well as the quality of images showed that EVs adhered best to fibronectin. Also, fibronectin gave the least background staining and was then chosen to be used for further experiments.

EVs adhered to fibronectin-coated slides were then imaged using a spinning disc confocal microscope [Figure 16]. IF images revealed CD63 positive membranous structures that were approximately within the range of 0.5 μm to 5 μm. Although some of the imaged structures appeared to have a spherical shape suggesting they could be a single large vesicle many of the imaged structures had a more irregular shape that could be interpreted as a clump of smaller vesicles that fall under the resolution limit of the microscope. The resolution of IF images doesn’t allow for detailed observations of EV structure and composition therefore to better delineate EV characteristics ExM was implemented.

The images captured in Figure 16 were primarily taken as a preparatory step for visualizing EVs using ExM. The main focus of the experiment was to visualize EVs derived from B cells, rather than to investigate their specific characteristics. As a result, important parameters such as size distribution were not quantified. However, the images still provide valuable preliminary information about the morphology of the EVs, which can be used as a basis for future studies aimed at characterizing these vesicles in more detail.

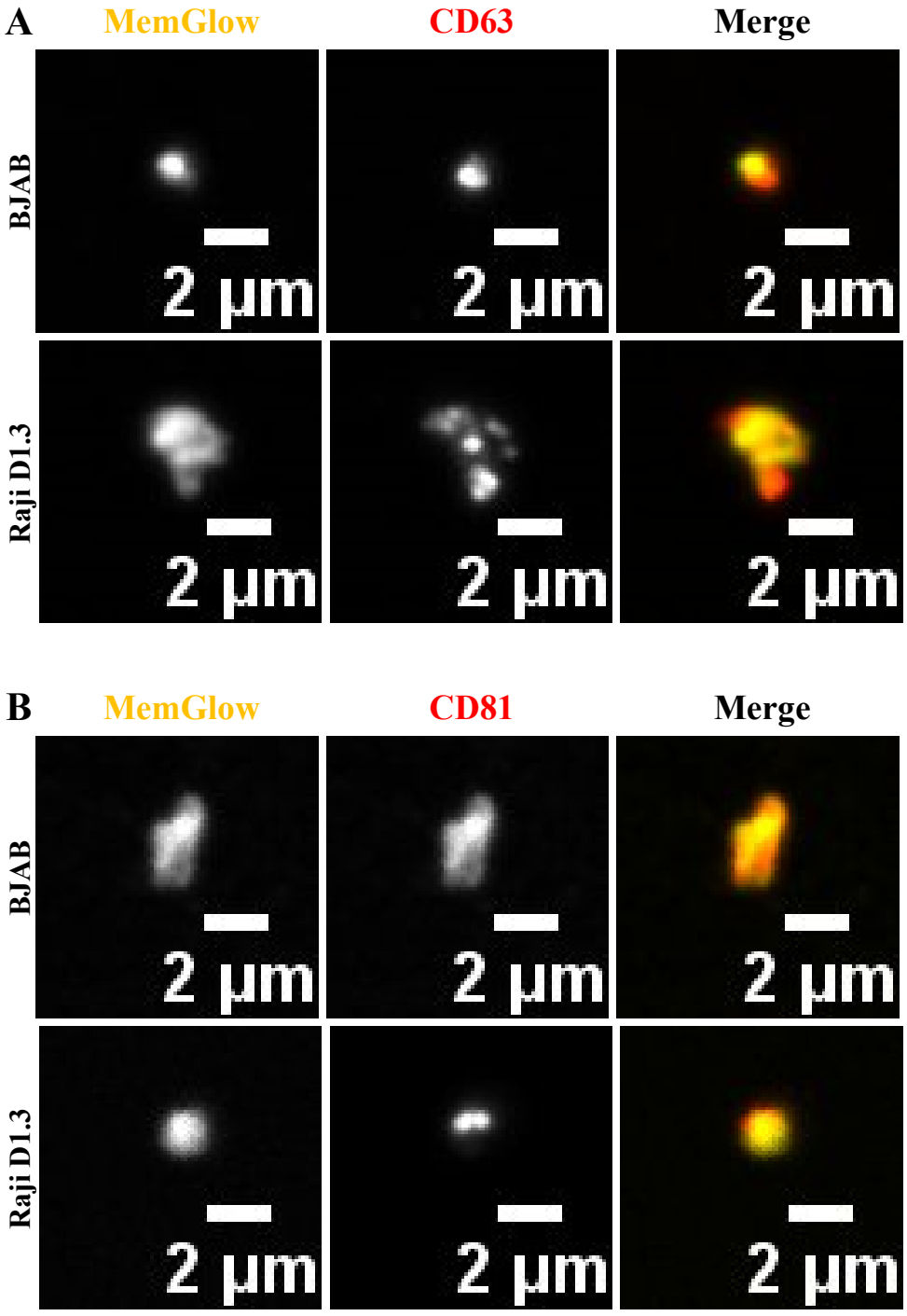

Figure 16 Immunofluorescence imaging of EVs on fibronectin. EVs were isolated, adhered to the fibronectin-coated slides, and stained**.** Images reveal irregular shapes and clumps with partial overlap of membrane and protein staining. Images are maximum intensity projections **(A)** EVs from activated Raji D1.3 and BJAB cell lines stained for CD63 and membrane (MemGlow) **(B)** EVs from non-activated Raji D1.3 and BJAB cell lines stained for CD81 and membrane (MemGlow)

4.3.3 Live cell staining with MembraneExM dye prior to EVs isolation

Imaging the EVs using ExM was done following the same protocol that was used for the ExM of the cells (see Chapter 4.2). This protocol requires fixing and staining the EVs after adhering them to the coverslip. However, membrane staining of the EVs can be done

either after fixing them on the coverslip or in the living cells, prior to EV isolation [Figure 17].

Staining the EVs prior to isolation allows for reducing the background noise from the membrane channel as the dye will not bind to the coverslip coating. However, to the best of our knowledge, Chrometra MembraneExM dye was never tested on living cells. To evaluate whether it is possible to stain the EVs prior to the isolation with MembraneExM dye, the dye was tested on living cells.

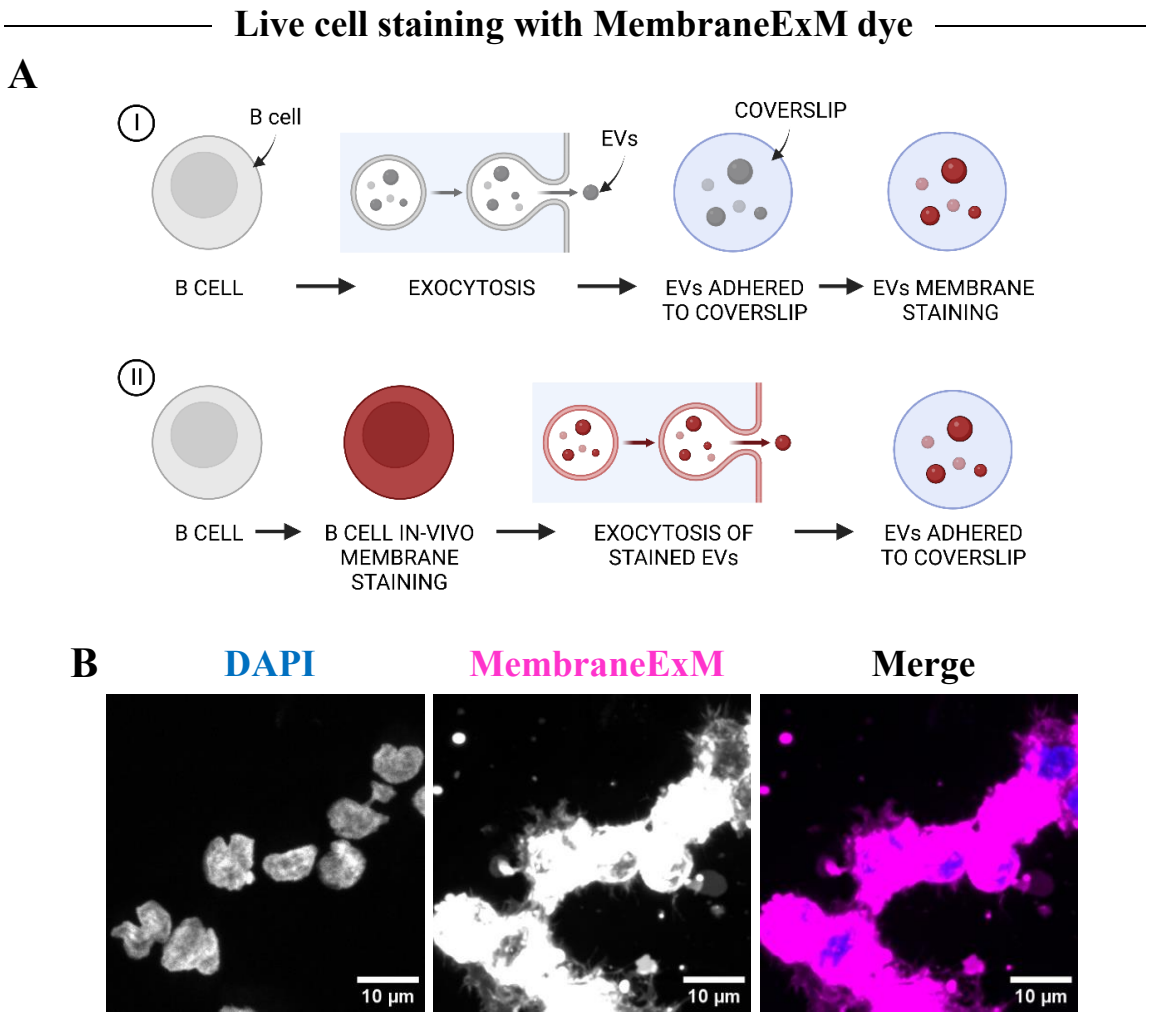

Figure 17 Live cell staining with MembraneExM dye. (A) Illustration of EVs staining procedure pre- and post-isolation I. Staining the EVs is done on the coverslip by incubating with a fluorescent probe **II.** Live cells are stained with a fluorescent probe which results in a release of EVs that are labeled prior to secretion. This image shows exocytosis as an example of how EVs can be secreted, however, it is important to note that other ways of EV secretion are possible. **(B)** The dye was incubated with Raji D1.3 non-activated cells, which were then fixed and imaged. Due to high signal intensity, the images were oversaturated despite minimizing the exposure time. Membrane dye was successfully internalized and no alterations in cell behavior were observed.

MembraneExM was added to the living cells medium in the same ratio as the one used for fixed sample staining. Cells were then incubated for 10 minutes at 37°C. After the incubation cells were centrifuged and resuspended in a cell culture medium. Cells were

then seeded on coated coverslips and incubated for 15 min at 37°C allowing them to adhere. Cells were then fixed and mounted for imaging.

IF imaging of live stained cells showed a very bright signal from the MembraneExM channel [Figure 17]. The signal intensity in the images was too strong, leading to oversaturation despite minimizing the exposure time. The results demonstrate that the dye was successfully internalized and stained the internal membranes of the cells, allowing for the secretion of pre-stained EVs. Furthermore, we observed that the cells adhered and appeared normal, indicating that the dye did not appear to be toxic within the 30-minute timeframe tested. For those reasons, we decided to use the EVs pre-stained with MembraneExM for the experiments focused on the development of the ExM of the EVs. However, due to limited knowledge of the exact effects of the dye on cellular behavior, experiments examining the biological behavior of cells and EVs should be carefully considered.

4.3.4 ExM enables high-resolution imaging of EVs adhered to fibronectin-coated substrates

After optimization of immunofluorescence microscopy sample preparation of EVs and pre-staining EVs with MembraneExM, the ExM protocol described in Chapter 4.2 was applied for EV samples. Isolated EVs were incubated on fibronectin, fixed, stained, and then subjected to the gelation and expansion process.

The volume yield, of isolated EVs, is relatively small and amounts to approximately 250 µl of EVs per condition. For this reason, to be able to efficiently use the EVs for different experiments, it is beneficial to use a possibly small volume of the isolated EVs per coverslip while adhering the EVs to the substrate. Two different techniques were tested and compared [Figure 18]. Method A consisted of placing the EVs on top of a fibronectin-coated coverslip. For the bubble to form 150 µl of EVs were needed. Coverslips were then incubated at room temperature on the mild shaker to increase the chance of EV binding. Method B consisted of placing a 50 µl drop of EVs on parafilm and then fibronectin-coated coverslip on top and incubating for two hours at room temperature. Both IF and ExM samples were prepared using the above methods in order to evaluate the quality of the obtained images. Although method B allows using fewer EVs volume, the amount of adhered EVs was smaller and samples had significantly more background staining. For the above reasons, method A was used for further experiments.

ExM of B cell derived EVs

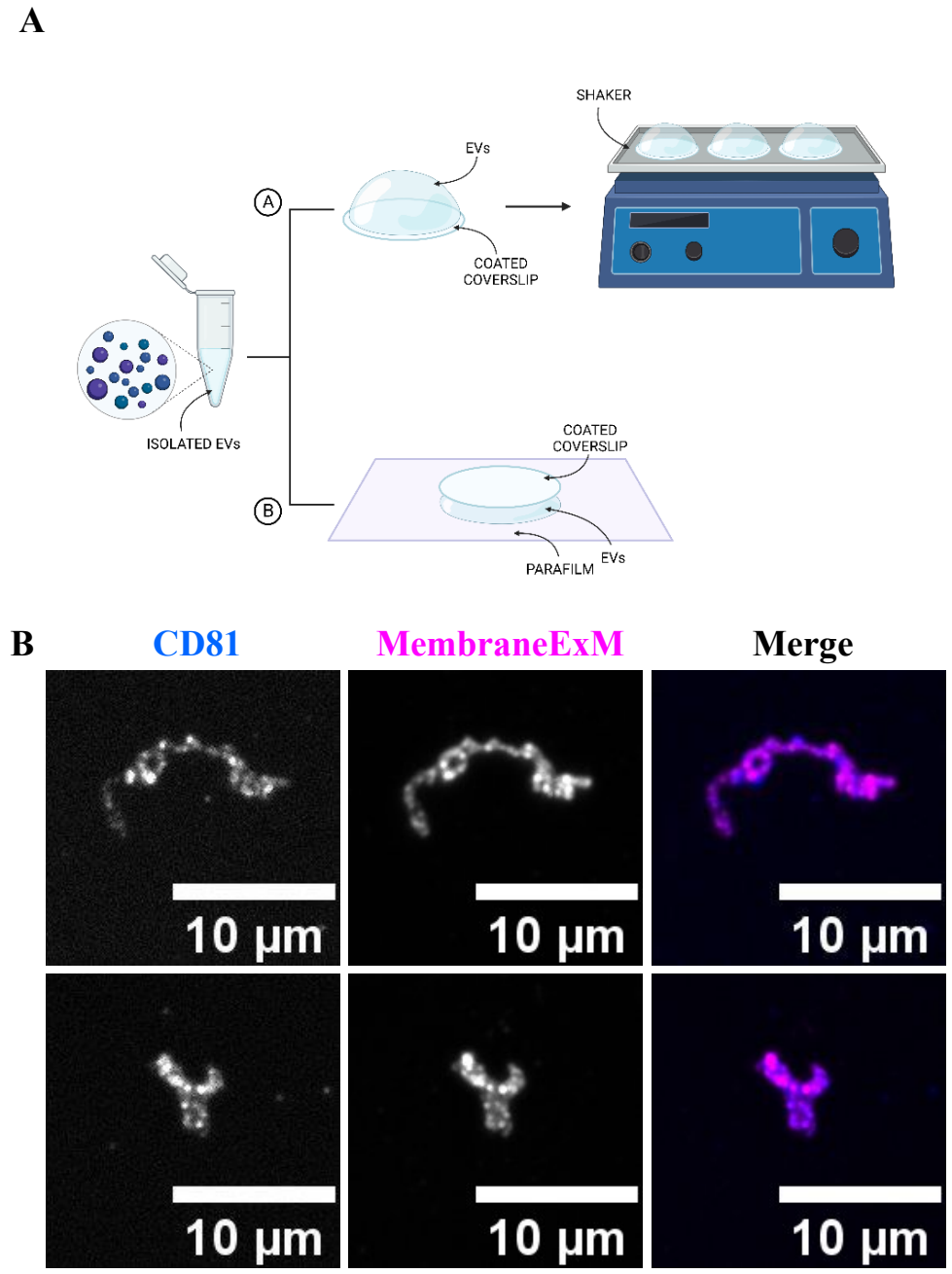

Figure 18 ExM of EVs derived from activated Raji D1.3 cells. (A) Schematic representation of EV adhesion techniques on fibronectin-coated coverslips. Method A. EVs are placed on top of the coverslip and incubated on a mild shaker to increase the chance of EV binding. Method B. EVs are placed on parafilm with a fibronectin-coated coverslip on top. Although method B requires to use smaller EV volume, method A results in less background noise and more adhered EVs. **(B)** Maximum intensity projections of two representative structures are shown. Isolated EVs were plated on coverslips, adhered to fibronectin, and incubated on the shaker prior to gelation. EVs were positive for CD81, which is a common EV marker. Membranous finger-like structures were observed during imaging. The **s**cale bar shows the size after expansion, not the actual size.

Imaging the EVs with ExM gave promising results [Figure 18], although the density of EVs in the gel decreased compared to IF samples potentially due to poor anchoring. EVs plated on coverslips and imaged with ExM were not entirely vesicular. Mostly, finger-like structures were observed with rounded vesicular structures being present. Similar aggregates were previously observed by electron microscopy in EVs isolated from human

brain tissue [89], muscle cells [90], and other sources. The staining revealed that the imaged structures were CD81 positive suggesting their vesicular nature, as CD81 is one of the commonly used EV markers. Control samples that underwent the same preparation and staining steps as the EV-containing samples but lacked EVs did not show similar structures. Thus, the structures observed were likely derived from the SEC-isolated EVs, leading to the conclusion that the images depict expanded EVs forming bigger aggregates.

In addition to MembraneExM dye, 20 nM MemGlow 488 was tested in the expansion. Using MemGlow gave an adequate signal, especially for EV staining.

4.3.5 ExM for imaging vesicles suspended in the gel volume

Using fibronectin-coated coverslips for EV imaging with ExM has certain limitations. In particular, only a fraction of EVs may successfully adhere to the coverslips, while others remain unattached, resulting in the loss of EVs during the process. Additionally, different EV subpopulations might exhibit different adhesion efficacy, which can compromise a reliable overview of the studied sample. Also, the use of frozen or fixed EVs is limited due to their inability to adhere to slide, which results in the need of using freshly isolated EVs for each experiment. To address this issue, a new method was developed where EVs are not attached to the coverslip prior to the gelation process, but instead, they are suspended in the volume of the gelation solution and anchored in the gel volume during the gel polymerization [Figure 19].

Before preparing the gelation solution containing EVs, the EVs were fixed and stained according to the following protocol. Isolated EVs were fixed by adding 4% PFA to the EV volume in a 1:3 PFA to EV ratio in order to obtain 1% PFA. Fixed EVs were then stained by adding fluorescent dyes or directly conjugated antibodies directly to the fixed EV volume. Staining was followed by the addition of AcX. EVs were incubated in AcX for at least one hour or overnight. We observed that longer AcX incubation resulted in better EV yield in the gel. The EVs prepared in this way were then used for monomer solution (MS) preparation. Usually, MS components are dissolved in PBS. Here, instead of using PBS, isolated EV samples were used as a medium for MS preparation. This allows incorporating all the EVs present in the sample into the hydrogel meshwork. Once the MS containing EVs was prepared, the rest of the sample preparation steps was the same as for the ExM protocol with EVs on the coverslips. The gelation solution was prepared from the monomer solution, and incubated in the gelation chambers. The protocol then continued until the expansion and imaging.

As opposed to typical IF sample preparation, the current study did not involve any washing steps. This was due to the fact that removing components such as PFA, dyes, and AcX from the sample volume would require procedures such as ultracentrifugation, which were not feasible for the current experimental setup as it would likely make the protocol too long and technically challenging and compromise the accessibility of ExM technique. For the above reason PFA, dyes, and AcX were not removed from the sample. Although this approach might result in compromised sample purity and introduce potential interference of additional components with the gelation solution, it allowed for a more efficient sample preparation procedure.

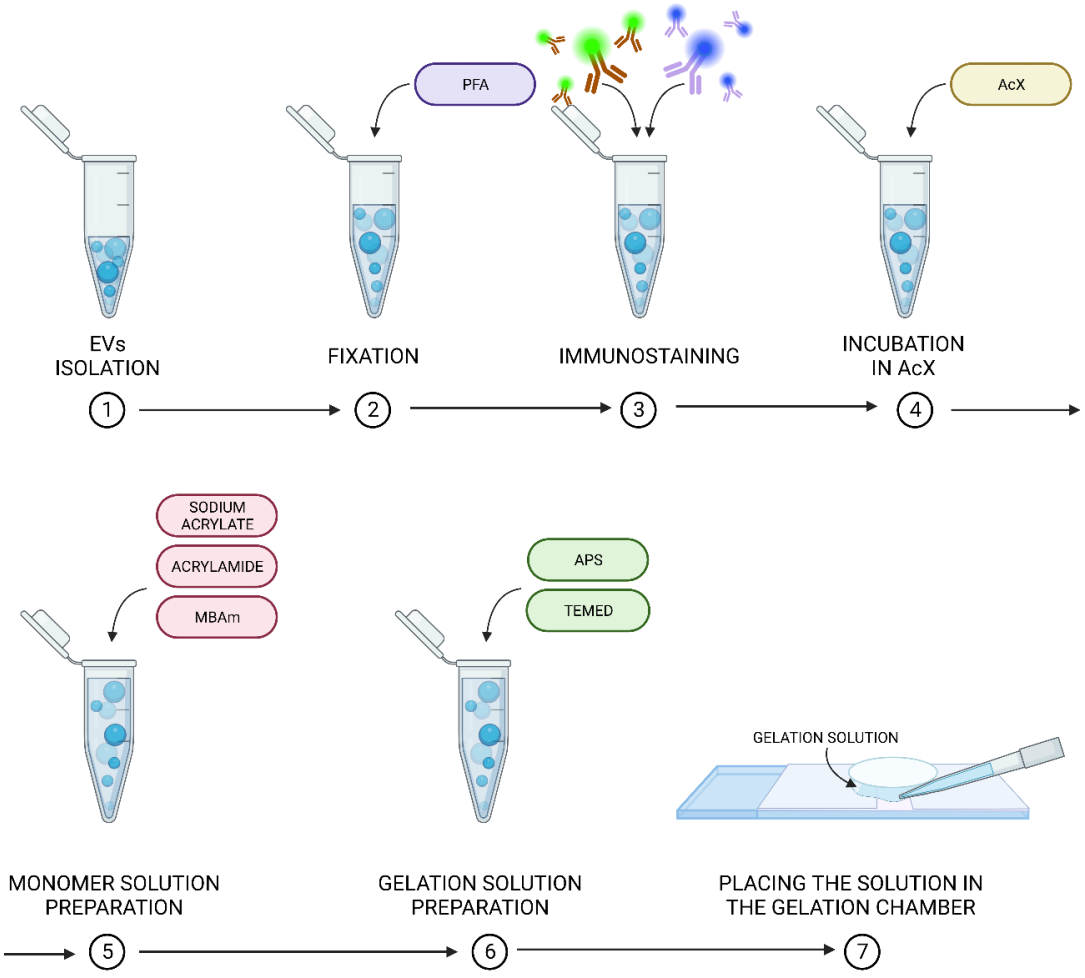

Figure 19 Gelation solution preparation workflow for ExM with EVs in the gel volume. Isolated EVs are fixed with PFA (1), stained using fluorescent probes or directly conjugated antibodies (2), and incubated in AcX to enable EV binding into the gel meshwork (3). Monomer solution components are dissolved in the EV solution (5) followed by the addition of APS and TEMED to create the gelation solution (6). The gelation solution is then pipetted into the gelation chamber (7). The coverslip is placed on top to ensure the appropriate size of the gel after the polymerization. Subsequent steps are identical to the previously described ExM protocol [Figure 12].

No major influence of those additional components on the formation of the gels was observed. However, in some of the experiments, the stiffness of the gels was compromised and their rigidity was reduced compared to those prepared using standard

methods. In some cases, the gels did not polymerize at all, which was an unexpected outcome given the consistent experimental conditions and using the same sample preparation protocol. Although it is possible that there were variations in the gel composition or the environmental conditions, it is difficult to determine the specific reasons that contributed to the inconsistencies in the outcome of the experiments without future investigation. Given that the rigidity and polymerization of the control samples, that did not contain the EVs, appeared similar to those that did, it can be concluded that the presence or absence of EVs did not significantly impact the observable properties of the gels. Nevertheless, we observed that increasing the concentration of all of the gelation solution components, that is sodium acrylate, acrylamide, MBAm, APS, and TEMED by a factor of 1.1 improved the rigidity of the gels. It was however not further investigated how the addition of the components such as PFA, and AcX to the gel volume, and the increase in the concentration of the gelation solution components affects the polymerization reaction and the uniformity of the expansion.

Due to the lack of washing steps in the sample preparation protocol, fluorescent dyes were not removed from the samples, however, this should not result in additional background staining. The sample preparation protocol was based on the protein retention ExM method, where AcX is used to modify the amines present in the proteins so that they can be incorporated into the gel together with the attached fluorophores. Therefore, those fluorescent molecules that did not bind to any proteins should not be incorporated into the gel. This was confirmed by imaging the samples that did not contain the EVs. No signal nor fluorophores aggregates were found in the control samples.

ExM with gel-suspended EVs gave promising results [Figure 20]. The quality of the images and the visualized structures resembled the ones imaged with EVs adhered to coverslips, however, more of bigger spherical structures were visible with this method. The size range of obtained structures was between 2 μm to 10μm, which after taking into account the gel expansion coefficient, calculated as a ratio between gel diameter before and after expansion, amounts to a size range between 200 nm to 1 μm. This fits into the size range of the EV population, which is between 30 nm to 5 μm.

Similarly to imaging the cells with ExM (see Chapter 4.2), we experienced hydrogel drift. For this reason, it was not always possible to acquire z-stacks of the EVs, which limits the amount of data characterizing the EV structure that we were able to acquire. Z-stack images are more insightful, especially due to the irregular morphology of the EVs, their non-spherical shapes, and the aggregates that their form.

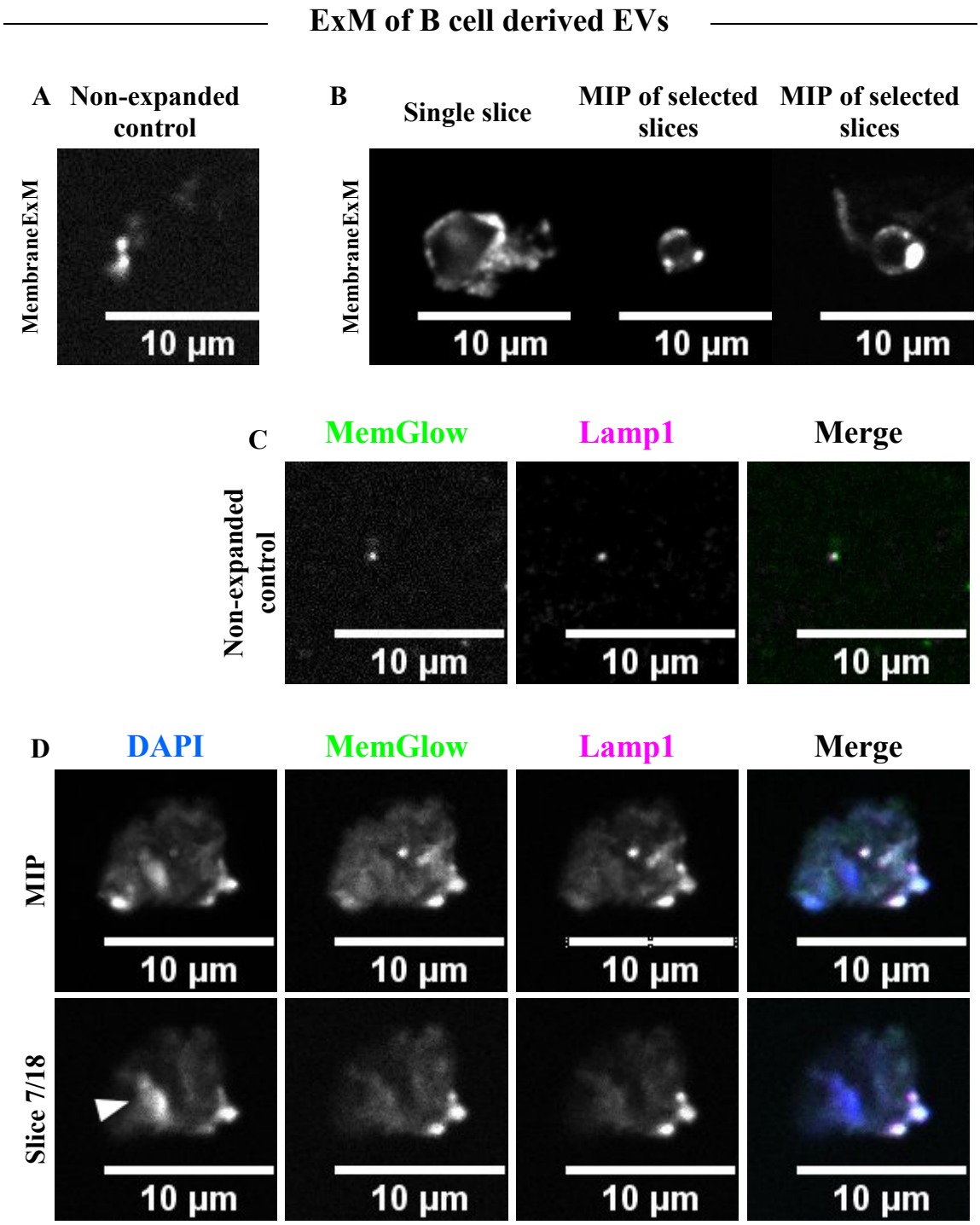

Figure 20 ExM of EVs derived from activated BJAB cells. (A) Non-expanded controls were used to observe the sizes of the EVs before the expansion, as well as to confirm that the staining worked successfully. Here, a representative single slice, showing EV stained with MembraneExM is shown. **(B)** Some of the imaged EVs were characterized by spherical morphology as seen in the membrane staining. Here, three different EVs are shown. Images are either a single slice or a maximum intensity projection (MIP). Those projections were chosen as they best reflect the spherical structure of the EVs **(C)** Non-expanded controls of a representative single slice, showing EV stained with MemGlow and Lamp1 is shown. **(D)** The surface of EVs is not always uniform and spherical but instead exhibits irregularities and pits, which appear as a ring-shaped morphology. Therefore, an accurate 3D representation of an EV can be challenging. Here, a 3D structure of an expanded EV is shown in both maximum intensity projection (MIP) and one selected slice. Although the size and distribution of different molecules are well visible using MIP, the details showing ring-like structures are lost. Showing single slices allows us to better visualize those structures. Arrows on the DAPI channel indicate regions with the strongest DAPI signal. Interestingly, we noticed that DAPI was often located in clumps on the edge of the vesicles.

In addition to vesicular markers such as CD63 and CD81, EVs were also stained with LAMP1. Although LAMP1 is a lysosomal marker, it was also identified in some of the extracellular vesicle populations [91]. Also, DAPI staining was used to visualize nucleic acids that can be carried by the EVs. DAPI staining is widely used with cells, as it targets double-stranded DNA, however, it is also possible to use it for targeting nucleic acids present in the EVs. Interestingly we noticed many EVs that were positive for DAPI staining. In those EVs, DAPI was not evenly distributed but localized in specific spots on the external membrane of the EVs [Figure 20]. The absence of fully overlapping signals between different stainings indicates that the observed signal is not a result of bleedthrough from other channels, but rather reflects genuine staining.

To visualize the EVs before the expansion, control samples were made [Figure 20]. After the incubation in AcX [Figure 19], stained EVs were placed on the coverslip and imaged using a spinning disc confocal microscope without binding them to the coverslip. As a result, significant movement of the EVs was observed, leading to some cases of blurred images. Nevertheless, these images still provided a representation of the EV scale prior to expansion.

Due to the high resolution of the images method can be used in the future to determine the structure of EVs with regard to the distribution of the proteins of interest. Even though the capacity of ExM to image multiple vesicles at once is limited, it permits the staining of multiple proteins of interest at once. In contrast, electron microscopy can be used to capture a high amount of EVs, however, it lacks the ability to selectively stain different molecules of interest. Therefore, these methods could effectively complement each other to provide a comprehensive overview of EV structure and molecular composition.

5 DISCUSSION

5.1 CHANGES IN INTRACELLULAR LOCALIZATION OF CD63 AND CD81 UPON B CELL ACTIVATION

Tetraspanins, including CD63 and CD81, are closely associated with intracellular vesicle trafficking as well as with extracellular vesicles [39], [42]. Therefore, labeling intracellular vesicles with tetraspanin markers can be used as an effective method for their visualization. As B cell activation is associated with various events, that can also affect vesicular trafficking of the cells, here, vesicular trafficking including tetraspanin-positive vesicles upon B cell activation was examined by analyzing the translocation of CD63 and CD81.

Based on preliminary microscopy observations, it was hypothesized that CD63 is predominantly present in the nucleus of non-activated B cells and translocates to the plasma membrane upon activation. For CD81, the hypothesis was that it is primarily localized on the plasma membrane in non-activated cells and translocates to the perinuclear area upon activation.

The distribution of CD81 and CD63 in non-activated and activated B cells was quantitatively assessed using immunofluorescence microscopy. The mean fluorescence intensity (MFI) of these tetraspanins was compared between the perinuclear area and cytoplasm using images acquired from a spinning disc confocal microscope. The Raji D1.3 and BJAB cell lines were used in the experiments. The analysis showed no significant difference in the localization of CD81 between activated and non-activated cells. In both cases, CD81 was located predominantly in the cytoplasm. However, in Raji D1.3 cells, a significant difference was observed for CD63, suggesting that CD63 translocates to the perinuclear area upon B cell activation. Those results were not expected based on the preliminary observations.

The translocation of CD63 and CD81 between the perinuclear area and the cytoplasm upon B cell activation could suggest their involvement in intracellular signaling pathways and antigen presentation, as well as the formation and release of extracellular vesicles. CD81 is known to play a role in B cells. It is present in the immune synapse, is involved in B cell signaling where it induces the activation of kinases such as Syk, is involved in the regulation of CD19 diffusion, and is a part of the B cell co-receptor complex. CD81 has been identified as one of the key proteins involved in the formation and release of

EVs, therefore a translocation of CD81 could have implications for the release of EVs and intracellular vesicle trafficking in B cells. However, the lack of significant difference in CD81 localization between activated and non-activated cells in this study suggests that its function may not be directly related to the translocation between the perinuclear area and the cytoplasm. Observed cytoplasmic localization of CD81 could be related to its role in EV biogenesis and secretion.

CD63 is a tetraspanin primarily located in intracellular compartments. It plays a role in the endosomal-lysosomal pathway, where it is involved in the sorting and trafficking of proteins and lipids. It has been shown that CD63 is involved in antigen presentation by B cells, which might be linked to increased exosome production upon CD63 depletion [40]. The translocation of CD63 towards the perinuclear area upon B cell activation could suggest that it is involved in antigen processing and presentation. The presence of CD63 in the perinuclear area might indicate that it's involved in protein sorting and transport or exosome release in activated B cells. Overall, the CD63 translocation upon B cell activation suggests that it may be an important regulator of intracellular signaling pathways, antigen presentation, and the formation and release of extracellular vesicles in B cells, however, those functions remain to be further investigated.

In this research, the quantification of tetraspanin localization was done based on the mean fluorescence intensity (MFI) of tetraspanin staining. For this purpose, a relatively simple segmentation method was utilized. However, there exist multiple image analysis tools and neural network approaches that enable image segmentation for studying tetraspanin translocation. A 2D segmentation of fixed cells was chosen also to fit within the timeframe of the project. However, as B cell activation is a process that can be observed within ten minutes from antigen binding, approaches such as live cell imaging could be implemented for *in-vivo* observation of CD63 and CD81 trafficking. It is also important to note that imaged cells were fixed after 15 minutes of activation time. The process of cell activation can vary across individual cells, leading to differing stages of activation even within the same sample. Furthermore, various cellular events may correspond to specific time points during activation. Hence, to get a more comprehensive understanding of CD63 and CD81 localization upon B cell activation *in-vivo* imaging approaches may be employed, or fixed samples may be imaged at multiple time points and compared. Such an approach would enable the observation of cellular events at different stages of B cell activation and facilitate a more complete analysis of the cellular process.

In this study, a middle plane of acquired z-stacks was chosen as a representative and quantified. It is however important to point out that although 2D analysis greatly simplifies the image analysis workflow, a single slide represents only a fraction of the acquired data. The outcome of the CD63 analysis was not consistent across the cell lines. In Raji D1.3 translocation to the perinuclear area was observed upon B cell activation, however, no significant changes in CD63 localization were in BJAB cells. As the results between the cell lines differ, the outcome of the analysis did not allow for clearly stating whether or not the translocation occurs upon B cell activation. The experiments should be repeated on other cell lines to further investigate this issue. It is however also possible that the differences in the results are caused by choosing a middle slice as a representative of CD63 distribution. A similar analysis as the one performed on the middle slice could be repeated on other planes, such as a middle plane. Additionally, 3D segmentation could provide more reliable data related to the entire cell rather than just a selected plane. Non-consistent results across the experiments might also indicate that the sample size is too small or that there is high variability in the measurements. It may be necessary to acquire more data to increase the power of the analysis and confirm the effect. Alternatively, different analysis methods may need to be employed to determine if other factors are affecting the results. It should also be noted that a more precise delineation of the perinuclear area for image analysis could be beneficial and provide more accurate results, however, it also presents additional image analysis challenges. The shape of B cells undergoes significant changes upon cell activation and spreading. The nucleus occupies most of the space in non-activated cells, while in activated cells there is a significant space between the nucleus and cell membrane where tetraspanins can localize. These morphological changes make it challenging to explicitly define the perinuclear area for studying protein localization.

5.2 Expansion Microscopy as a tool for visualizing intracellular vesicles of B cells

To visualize intracellular vesicles and better delineate CD63 and CD81 distribution in activated and non-activated B cells we implemented the expansion microscopy (ExM) technique. ExM allows for super-resolution imaging using diffraction-limited microscopes by physically expanding the sample, therefore it has a great potential for imaging vesicles that often fall under the resolution limit of the light microscope.

Here, the protein retention ExM protocol was optimized to be used with B cells. ExM imaging of B cells provided enhanced resolution as compared to the standard confocal microscope and allowed for clear visualization of vesicular structures within a cell. ExM was used to image the intracellular localization of CD63 in non-activated and activated Raji D1.3 cells, however, the number of cells imaged was not sufficient to give a representative overview of imaged cell population and to be quantified. Nevertheless, we observed that in all imaged non-activated cells CD63 was observed to localize predominantly in the cytoplasm, and in the majority of imaged activated cells CD63 localized predominantly in the perinuclear area, which is in agreement with the quantification of CD63 localization done using IF images. It is however important to remember that the assessment of CD63 intracellular localization was done through a visual examination of images, with no measurement taken.

In this study, ExM showed great potential for qualitative analysis. It provided an improved resolution and achieved high-quality staining of the samples, resulting in a clear visualization of all the imaged structures. The results from the ExM images showed changes in CD63 localization supporting the results of image analysis performed on non-expanded cells. Although the expansion factor of the gel varied across different experiments from around five-fold to ten-fold expansion the images can be a subject of further analysis. The reason why the gels did not fully expand in some of the cases is not clear, although a potential reason might be a not sufficient incubation time in MQ water before the imaging. Also, an insufficient amount of water left for incubation can result in the gel not fully expanding or shrinking. Differences in expansion factor affect the resolution of acquired images, therefore it is important to prevent the gel from not fully expanding in further experiments.

Preparing ExM is a more laborious and time-consuming process than IF sample preparation. It would therefore be advantageous to optimize the method in such a way that the maximum number of cells can be imaged in a single experiment. This would enable the acquisition of sufficient data for subsequent quantitative analysis, increasing the value of the study. Encountered problems that limited the number of acquired images were a small number of cells in the gel and hydrogel drift. In protein retention ExM, acryloyl-X (AcX) is used to anchor the proteins from the sample into the polymer meshwork. Therefore, the sample's ability to be incorporated into the gel depends solely on the successful incubation in AcX. It may be advantageous in the future, to optimize the AcX incubation step, especially with regard to concentration, as this could potentially

increase the number of amines that will be modified and incorporated into the gel, therefore increasing the number of cells that successfully bind into the gel.

Hydrogel drift is an issue that occurred while imaging some of the samples. This issue refers to a situation in which sample movement is observed causing sample blurring and image distortion. It results in channels not overlapping in a single plane as well as the z-stack slice's position being shifted. Different approaches have been developed, especially for live imaging, that can compensate for the drift, such as, for instance, Deep-Z [92] or the recently developed Fast4Dreg [93]. Although such image processing tools could be in the future used to correct hydrogel drift, in some cases the observed sample drift was so rapid, that it resulted in the cell moving outside of the field of view during imaging. Therefore there is still a need for limiting the drift during the acquisition process, to be able to capture the whole volume of the cell.

Before the imaging, samples were mounted in cell imaging chambers on Poly-L-Lysine coated slides. One of the aims of mounting in ExM is to prevent samples from drifting. Established ExM protocols suggest different types of sample holders, such as coverslips or Petri dishes. For longer imaging, physically attaching the sample to the holder is recommended. Described methods include coating the sample holder in Poly-L-Lysine, agarose, or even superglue [94]. In our case, Poly-L-Lysine wasn’t enough to prevent the drift. The remaining methods, that is agarose and superglue, are not suitable for the imaging setup where the imaging is done through the sample holder, therefore could not be implemented. However, there exist other solutions that aim to prevent the drift. In some of the research, samples were re-embedded in charge-neutral polyacrylamide gel [86], [88]. Although this method reduces the drift, it also causes a size reduction of the gel to approximately 70% of the initial expanded size. It might also cause a partial degradation of the fluorescent dyes. Additionally, it is also possible to functionalize the coverslips with acrydite via glass silanization before mounting re-embedded gels [87]. The re-embedding of the sample could possibly help in reducing the hydrogel drift in the future, therefore it is worth implementing in subsequent studies.

5.3 A NOVEL APPROACH TO EV IMAGING USING EXPANSION MICROSCOPY

Imaging the EVs brings additional challenges due to their nanoscopic size range. EVs are often visualized using electron microscopy (EM), as it provides good resolution and allows to image high number of EVs. However, as opposed to immunofluorescence microscopy, EM doesn’t allow for the simultaneous choice of multiple fluorophores.

Other super-resolution microscopes are being developed that aim to help with EV visualization, such as ONI Nanoimager, which enables EV visualization with dSTORM [95]. However, such solutions require specialized equipment and expertise which reduces their accessibility. Here, ExM was implemented to study EVs using a spinning disc confocal microscope.

The method developed in this study involves suspending the EVs within the gel volume instead of adhering them to the coverslips as in the standard ExM protocol. The isolated EVs were fixed with PFA and stained with directly conjugated antibodies and dyes that were added directly to the isolated EVs volume. Then, AcX was added to the stained EVs to allow protein binding to the gel meshwork. These prepared EVs were then utilized for monomer solution (MS) preparation. Typically, MS components are dissolved in PBS, but instead of PBS, the isolated EV samples were used as a medium for MS preparation. After the MS was prepared, the gelation solution (GS) was made by adding APS and TEMED. Then, the GS was polymerized, followed by expansion in MQ water. This resulted in an expanded gel with fluorescent-labeled EVs distributed throughout the entire volume of the gel. This approach gave promising results. We obtained super-resolution images of round, vesicular structures that were positive for both membrane and vesicular marker staining. No such structures were observed in the control samples. Furthermore, the size range of the structures that were imaged was consistent with the known size range of EVs, suggesting that the imaged structures were indeed EVs.

One of the major challenges associated with imaging EVs is the ability to accurately identify the presence of EVs within a given sample. Due to the heterogeneity of the EV population, it is difficult to precisely determine their morphology and distinguish them from other structures and cellular debris. As a result, it is crucial to confirm the presence of EVs in the sample prior to imaging, as well as implement strategies to ensure that the structures being observed are indeed EVs. The lack of markers that would be characteristic only for EVs makes it additionally challenging. In this study, Western blot analysis was conducted to confirm the presence of vesicular markers. EZRIN, CD81, and cathepsin S were present in all of the isolated EV samples, which indicates the presence of EVs in the samples. However, such analysis doesn’t exclude the presence of contaminants. International Society for Extracellular Vesicles (ISEV) suggests that the presence of principal components of structures other than EVs, which often can be co-isolated, should be checked in order to evaluate the purity of the sample [96]. For example, albumin can be used as a negative marker for EVs derived from cells that were cultured

with bovine serum. Such controls could be used in future studies to ensure that sample contaminants are not confused with EVs during imaging.

The gel preparation protocol described in this thesis didn't include washing steps, which means that sample preparation components such as PFA, fluorescent dyes, and AcX are not being removed. Also, some issues with gel polymerization and rigidity were observed during method development. In order to ensure that the modified protocol doesn't cause any distortions or anisotropies and that the gel expands uniformly, additional tools such as GelMap could be implemented [97]. This recently developed tool allows us to easily assess those properties and has great potential to be used as quality control. GelMap can be easily incorporated into the protocol by generating a fluorescent grid pattern on the coverslip using photolithography. The pattern would then be incorporated into the gel and expanded, acting as a reference. This tool would be highly beneficial for the evaluation of ExM protocol with EVs suspended in the gel volume.

Additionally, the prolonged exposure of EVs to PFA and AcX, and the consequences of not removing them could be further investigated to ensure that the structural integrity of EVs is not compromised by the presence of these components.

Even though further studies need to be done on visualizing EVs using ExM, this method has shown to have great potential to be used for EV imaging. Implementing this method can help to differentiate the EV population of B cells or any other small cell types such as e.g. T cells. Although, due to the lack of washing steps, currently only directly conjugated antibodies have been used, optimizing the process for staining with primary and secondary antibodies would make the method more versatile. Tools such as Exosome Spin Columns are commercially available and have been used to remove unincorporated dye from exosome labeling experiments [98]. Incorporating them into the workflow could significantly improve EV staining.

6 CONCLUSION

Multiple events are associated with B cell activation, yet many of them remain unexplored. This thesis focused on investigating intra- and extracellular vesicles of B cells upon activation. First, the translocation of tetraspanins CD63 and CD81 between the cytoplasm and perinuclear area were investigated. Based on preliminary observations it was hypothesized that in activated B cells CD63 translocates towards the plasma membrane and CD81 towards the perinuclear area. However, the results showed that CD63 translocates to the perinuclear area upon B cell activation in Raji D1.3 cells. No translocation was observed on the BJAB cell line. Also, no alterations in the cellular localization of CD81 were observed, which remained predominantly in the cytoplasm. Due to the inconsistent results between the two cell lines, and possible inaccuracies of chosen image analysis workflow, further analysis needs to be done to validate how B cell activation alters the trafficking of CD63 and CD81.

Expansion microscopy (ExM) was successfully implemented to study CD63 and CD81 positive vesicles in activated and non-activated B cells. Although the throughput of this method didn't allow for quantitative analysis of acquired images, this method allowed for high-resolution imaging suitable for qualitative description of observed B cell phenotypes.

The last part of the thesis focused on implementing expansion microscopy to study B cell-derived EVs. To the best of our knowledge EVs were not yet studied using ExM. We developed a method where EVs are added directly to the gelation solution so that they are suspended in the volume of the gel after polymerization. We demonstrate that this method allows for super-resolution EV imaging using different fluorescent labels. However, further studies should be done to ensure the reliability and uniformity of gel expansion and to validate the common marker stainings. In the future, this method can be implemented to help differentiate the B cell EV population. EVs have the potential to serve as biomarkers for various diseases, and consequently, tools such as the EV ExM method developed in this study are highly sought after for investigating EV structure and function.

7 ACKNOWLEDGMENTS

I would like to express my gratitude to my supervisors Pieta Mattila and Saara Hämälistö for giving me the opportunity to conduct my master's thesis project in the Lymphocyte Activation Lab, and for their guidance and support. I would also like to thank all of the lab members for their advice and insights, especially Amna for her help in the lab. Finally, I would like to thank my friends, boyfriend, and family for their understanding, support, and time, which helped me during the process of writing the thesis.

8 REFERENCES

[1] J. Parkin and B. Cohen, “An overview of the immune system,” *The Lancet*, vol. 357, no. 9270, pp. 1777–1789, Jun. 2001, doi: 10.1016/S0140-6736(00)04904-7.

[2] L. B. Nicholson, “The immune system,” *Essays Biochem*, vol. 60, no. 3, pp. 275–301, Oct. 2016, doi: 10.1042/EBC20160017.

[3] M. F. Flajnik and M. Kasahara, “Origin and evolution of the adaptive immune system: genetic events and selective pressures,” *Nat Rev Genet*, vol. 11, no. 1, pp. 47–59, Jan. 2010, doi: 10.1038/nrg2703.

[4] B. Beutler, “Innate immunity: an overview,” *Molecular Immunology*, vol. 40, no. 12, pp. 845–859, Feb. 2004, doi: 10.1016/j.molimm.2003.10.005.

[5] J. S. Marshall, R. Warrington, W. Watson, and H. L. Kim, “An introduction to immunology and immunopathology,” *Allergy, Asthma & Clinical Immunology*, vol. 14, no. 2, p. 49, Sep. 2018, doi: 10.1186/s13223-018-0278-1.

[6] B. Briney and J. Crowe, “Secondary mechanisms of diversification in the human antibody repertoire,” *Frontiers in Immunology*, vol. 4, 2013, Accessed: Jan. 22, 2023. [Online]. Available: https://www.frontiersin.org/articles/10.3389/fimmu.2013.00042

[7] P.-L. Chiu, C.-H. Chang, Y.-L. Lin, P.-H. Tsou, and B.-R. Li, “Rapid and Safe Isolation of Human Peripheral Blood B and T Lymphocytes through Spiral Microfluidic Channels,” *Sci Rep*, vol. 9, no. 1, Art. no. 1, May 2019, doi: 10.1038/s41598-019-44677-3.

[8] H. Eibel, H. Kraus, H. Sic, A.-K. Kienzler, and M. Rizzi, “B cell Biology: An Overview,” *Curr Allergy Asthma Rep*, vol. 14, no. 5, p. 434, May 2014, doi: 10.1007/s11882-014-0434-8.

[9] K. Pieper, B. Grimbacher, and H. Eibel, “B-cell biology and development,” *Journal of Allergy and Clinical Immunology*, vol. 131, no. 4, pp. 959–971, Apr. 2013, doi: 10.1016/j.jaci.2013.01.046.

[10] M.-I. Yuseff, P. Pierobon, A. Reversat, and A.-M. Lennon-Duménil, “How B cells capture, process and present antigens: a crucial role for cell polarity,” *Nat Rev Immunol*, vol. 13, no. 7, Art. no. 7, Jul. 2013, doi: 10.1038/nri3469.

[11] E. Kuokkanen, V. Šuštar, and P. K. Mattila, “Molecular Control of B Cell Activation and Immunological Synapse Formation,” *Traffic*, vol. 16, no. 4, pp. 311–326, 2015, doi: 10.1111/tra.12257.

[12] S. J. Fleire, J. P. Goldman, Y. R. Carrasco, M. Weber, D. Bray, and F. D. Batista, “B Cell Ligand Discrimination Through a Spreading and Contraction Response,” *Science*, vol. 312, no. 5774, pp. 738–741, May 2006, doi: 10.1126/science.1123940.

[13] S. Pal Singh, F. Dammeijer, and R. W. Hendriks, “Role of Bruton’s tyrosine kinase in B cells and malignancies,” *Mol Cancer*, vol. 17, p. 57, Feb. 2018, doi: 10.1186/s12943-018-0779-z.

[14] D. G. Efremov, S. Turkalj, and L. Laurenti, “Mechanisms of B Cell Receptor Activation and Responses to B Cell Receptor Inhibitors in B Cell Malignancies,” *Cancers (Basel)*, vol. 12, no. 6, p. 1396, May 2020, doi: 10.3390/cancers12061396.

[15] A. M. Bogusz *et al.*, “Quantitative Immunofluorescence Reveals the Signature of Active B-cell Receptor Signaling in Diffuse Large B-cell Lymphoma,” *Clinical Cancer Research*, vol. 18, no. 22, pp. 6122–6135, Nov. 2012, doi: 10.1158/1078-0432.CCR-12-0397.

[16] A. A. Cabrera-Ortega, D. Feinberg, Y. Liang, C. Rossa, and D. T. Graves, “The Role of Forkhead Box 1 (FOXO1) in the Immune System: Dendritic Cells, T Cells,

B Cells, and Hematopoietic Stem Cells," *Crit Rev Immunol*, vol. 37, no. 1, pp. 1–13, 2017, doi: 10.1615/CritRevImmunol.2017019636.

[17] P. Simeone *et al.*, "Extracellular Vesicles as Signaling Mediators and Disease Biomarkers across Biological Barriers," *Int J Mol Sci*, vol. 21, no. 7, p. 2514, Apr. 2020, doi: 10.3390/ijms21072514.

[18] G. van Niel, D. R. F. Carter, A. Clayton, D. W. Lambert, G. Raposo, and P. Vader, "Challenges and directions in studying cell–cell communication by extracellular vesicles," *Nat Rev Mol Cell Biol*, vol. 23, no. 5, Art. no. 5, May 2022, doi: 10.1038/s41580-022-00460-3.

[19] G. van Niel, G. D'Angelo, and G. Raposo, "Shedding light on the cell biology of extracellular vesicles," *Nat Rev Mol Cell Biol*, vol. 19, no. 4, pp. 213–228, Apr. 2018, doi: 10.1038/nrm.2017.125.

[20] L. Ma *et al.*, "Discovery of the migrasome, an organelle mediating release of cytoplasmic contents during cell migration," *Cell Res*, vol. 25, no. 1, Art. no. 1, Jan. 2015, doi: 10.1038/cr.2014.135.

[21] D. K. Jeppesen, Q. Zhang, J. L. Franklin, and R. J. Coffey, "Extracellular vesicles and nanoparticles: emerging complexities," *Trends in Cell Biology*, Feb. 2023, doi: 10.1016/j.tcb.2023.01.002.

[22] H. Valadi, K. Ekström, A. Bossios, M. Sjöstrand, J. J. Lee, and J. O. Lötvall, "Exosome-mediated transfer of mRNAs and microRNAs is a novel mechanism of genetic exchange between cells," *Nat Cell Biol*, vol. 9, no. 6, Art. no. 6, Jun. 2007, doi: 10.1038/ncb1596.

[23] L. Cheng and A. F. Hill, "Therapeutically harnessing extracellular vesicles," *Nat Rev Drug Discov*, vol. 21, no. 5, Art. no. 5, May 2022, doi: 10.1038/s41573-022-00410-w.

[24] Susannah Hallal, Ágota Tűzesi, Georges E. Grau, Michael E. Buckland, and Kimberley L. Alexander, "Understanding the extracellular vesicle surface for clinical molecular biology," *Journal of extracellular vesicles*, 2022, doi: 10.1002/jev2.12260.

[25] J. S. Brzozowski *et al.*, "Lipidomic profiling of extracellular vesicles derived from prostate and prostate cancer cell lines," *Lipids in Health and Disease*, vol. 17, no. 1, p. 211, Sep. 2018, doi: 10.1186/s12944-018-0854-x.

[26] E. van der Pol, A. N. Böing, P. Harrison, A. Sturk, and R. Nieuwland, "Classification, Functions, and Clinical Relevance of Extracellular Vesicles," *Pharmacol Rev*, vol. 64, no. 3, pp. 676–705, Jul. 2012, doi: 10.1124/pr.112.005983.

[27] E. I. Buzás, E. Á. Tóth, B. W. Sódar, and K. É. Szabó-Taylor, "Molecular interactions at the surface of extracellular vesicles," *Semin Immunopathol*, vol. 40, no. 5, pp. 453–464, 2018, doi: 10.1007/s00281-018-0682-0.

[28] J. Kowal *et al.*, "Proteomic comparison defines novel markers to characterize heterogeneous populations of extracellular vesicle subtypes," *Proc Natl Acad Sci U S A*, vol. 113, no. 8, pp. E968–E977, Feb. 2016, doi: 10.1073/pnas.1521230113.

[29] L. M. Doyle and M. Z. Wang, "Overview of Extracellular Vesicles, Their Origin, Composition, Purpose, and Methods for Exosome Isolation and Analysis," *Cells*, vol. 8, no. 7, p. 727, Jul. 2019, doi: 10.3390/cells8070727.

[30] T. Yadati, T. Houben, A. Bitorina, and R. Shiri-Sverdlov, "The Ins and Outs of Cathepsins: Physiological Function and Role in Disease Management," *Cells*, vol. 9, no. 7, p. 1679, Jul. 2020, doi: 10.3390/cells9071679.

[31] M. M. Mohamed and B. F. Sloane, "multifunctional enzymes in cancer," *Nat Rev Cancer*, vol. 6, no. 10, Art. no. 10, Oct. 2006, doi: 10.1038/nrc1949.

[32] P. Smyth, J. Sasiwachirangkul, R. Williams, and C. J. Scott, "Cathepsin S (CTSS) activity in health and disease - A treasure trove of untapped clinical

potential," *Molecular Aspects of Medicine*, vol. 88, p. 101106, Dec. 2022, doi: 10.1016/j.mam.2022.101106.

[33] R. D. A. Wilkinson, R. Williams, C. J. Scott, and R. E. Burden, "Cathepsin S: therapeutic, diagnostic, and prognostic potential," *Biological Chemistry*, vol. 396, no. 8, pp. 867–882, Aug. 2015, doi: 10.1515/hsz-2015-0114.

[34] M. Adada, D. Canals, Y. A. Hannun, and L. M. Obeid, "Sphingolipid regulation of ezrin, radixin, and moesin proteins family: Implications for cell dynamics," *Biochimica et Biophysica Acta (BBA) - Molecular and Cell Biology of Lipids*, vol. 1841, no. 5, pp. 727–737, May 2014, doi: 10.1016/j.bbalip.2013.07.002.

[35] S. Charrin, S. Jouannet, C. Boucheix, and E. Rubinstein, "Tetraspanins at a glance," *Journal of Cell Science*, vol. 127, no. 17, pp. 3641–3648, Sep. 2014, doi: 10.1242/jcs.154906.

[36] V. Toribio and M. Yáñez-Mó, "Tetraspanins interweave EV secretion, endosomal network dynamics and cellular metabolism," *European Journal of Cell Biology*, vol. 101, no. 3, p. 151229, Jun. 2022, doi: 10.1016/j.ejcb.2022.151229.

[37] Z. Andreu and M. Yáñez-Mó, "Tetraspanins in Extracellular Vesicle Formation and Function," *Frontiers in Immunology*, vol. 5, 2014, Accessed: Sep. 23, 2022. [Online]. Available: https://www.frontiersin.org/articles/10.3389/fimmu.2014.00442

[38] Y. Huang and L. Yu, "Tetraspanin-enriched microdomains: The building blocks of migrasomes," *Cell Insight*, vol. 1, no. 1, p. 100003, Feb. 2022, doi: 10.1016/j.cellin.2021.100003.

[39] M. S. Pols and J. Klumperman, "Trafficking and function of the tetraspanin CD63," *Exp Cell Res*, vol. 315, no. 9, pp. 1584–1592, May 2009, doi: 10.1016/j.yexcr.2008.09.020.

[40] S. H. Petersen, E. Odintsova, T. A. Haigh, A. B. Rickinson, G. S. Taylor, and F. Berditchevski, "The role of tetraspanin CD63 in antigen presentation via MHC class II," *European Journal of Immunology*, vol. 41, no. 9, pp. 2556–2561, 2011, doi: 10.1002/eji.201141438.

[41] M. W. J. Wentink, M. C. van Zelm, J. J. M. van Dongen, K. Warnatz, and M. van der Burg, "Deficiencies in the CD19 complex," *Clinical Immunology*, vol. 195, pp. 82–87, Oct. 2018, doi: 10.1016/j.clim.2018.07.017.

[42] S. Levy, "Function of the tetraspanin molecule CD81 in B and T cells," *Immunol Res*, vol. 58, no. 2, pp. 179–185, May 2014, doi: 10.1007/s12026-014-8490-7.

[43] P. K. Mattila *et al.*, "The Actin and Tetraspanin Networks Organize Receptor Nanoclusters to Regulate B Cell Receptor-Mediated Signaling," *Immunity*, vol. 38, no. 3, pp. 461–474, Mar. 2013, doi: 10.1016/j.immuni.2012.11.019.

[44] G. Berumen Sánchez, K. E. Bunn, H. H. Pua, and M. Rafat, "Extracellular vesicles: mediators of intercellular communication in tissue injury and disease," *Cell Communication and Signaling*, vol. 19, no. 1, p. 104, Oct. 2021, doi: 10.1186/s12964-021-00787-y.

[45] S. Nair and C. Salomon, "Extracellular vesicles and their immunomodulatory functions in pregnancy," *Semin Immunopathol*, vol. 40, no. 5, pp. 425–437, Sep. 2018, doi: 10.1007/s00281-018-0680-2.

[46] G. Raposo *et al.*, "B lymphocytes secrete antigen-presenting vesicles.," *Journal of Experimental Medicine*, vol. 183, no. 3, pp. 1161–1172, Mar. 1996, doi: 10.1084/jem.183.3.1161.

[47] A. Muntasell, A. C. Berger, and P. A. Roche, "T cell-induced secretion of MHC class II–peptide complexes on B cell exosomes," *EMBO J*, vol. 26, no. 19, pp. 4263–4272, Oct. 2007, doi: 10.1038/sj.emboj.7601842.

[48] E. Panagiotou, N. K. Syrigos, A. Charpidou, E. Kotteas, and I. A. Vathiotis, "CD24: A Novel Target for Cancer Immunotherapy," *J Pers Med*, vol. 12, no. 8, p. 1235, Jul. 2022, doi: 10.3390/jpm12081235.
[49] D. C. Ayre *et al.*, "CD24 induces changes to the surface receptors of B cell microvesicles with variable effects on their RNA and protein cargo," *Sci Rep*, vol. 7, no. 1, Art. no. 1, Aug. 2017, doi: 10.1038/s41598-017-08094-8.
[50] H.-D. Phan *et al.*, "CD24 and IgM Stimulation of B Cells Triggers Transfer of Functional B Cell Receptor to B Cell Recipients Via Extracellular Vesicles," *J Immunol*, vol. 207, no. 12, pp. 3004–3015, Dec. 2021, doi: 10.4049/jimmunol.2100025.
[51] T. Kato, J. F. Fahrmann, S. M. Hanash, and J. Vykoukal, "Extracellular Vesicles Mediate B Cell Immune Response and Are a Potential Target for Cancer Therapy," *Cells*, vol. 9, no. 6, Art. no. 6, Jun. 2020, doi: 10.3390/cells9061518.
[52] M. P. Oksvold *et al.*, "Expression of B-Cell Surface Antigens in Subpopulations of Exosomes Released From B-Cell Lymphoma Cells," *Clinical Therapeutics*, vol. 36, no. 6, pp. 847-862.e1, Jun. 2014, doi: 10.1016/j.clinthera.2014.05.010.
[53] C. Admyre *et al.*, "B cell–derived exosomes can present allergen peptides and activate allergen-specific T cells to proliferate and produce TH2-like cytokines," *Journal of Allergy and Clinical Immunology*, vol. 120, no. 6, pp. 1418–1424, Dec. 2007, doi: 10.1016/j.jaci.2007.06.040.
[54] S. K. Lundy, M. W. Klinker, and D. A. Fox, "Killer B Lymphocytes and Their Fas Ligand Positive Exosomes as Inducers of Immune Tolerance," *Frontiers in Immunology*, vol. 6, 2015, Accessed: Feb. 20, 2023. [Online]. Available: https://www.frontiersin.org/articles/10.3389/fimmu.2015.00122
[55] S. C. Saunderson, A. C. Dunn, P. R. Crocker, and A. D. McLellan, "CD169 mediates the capture of exosomes in spleen and lymph node," *Blood*, vol. 123, no. 2, pp. 208–216, Jan. 2014, doi: 10.1182/blood-2013-03-489732.
[56] M. Yáñez-Mó *et al.*, "Biological properties of extracellular vesicles and their physiological functions," *J Extracell Vesicles*, vol. 4, p. 10.3402/jev.v4.27066, May 2015, doi: 10.3402/jev.v4.27066.
[57] R. J. Lobb *et al.*, "Optimized exosome isolation protocol for cell culture supernatant and human plasma," *Journal of Extracellular Vesicles*, vol. 4, no. 1, p. 27031, Jan. 2015, doi: 10.3402/jev.v4.27031.
[58] L. Dong *et al.*, "Comprehensive evaluation of methods for small extracellular vesicles separation from human plasma, urine and cell culture medium," *Journal of Extracellular Vesicles*, vol. 10, no. 2, p. e12044, 2020, doi: 10.1002/jev2.12044.
[59] A. Gámez-Valero, M. Monguió-Tortajada, L. Carreras-Planella, M. Franquesa, K. Beyer, and F. E. Borràs, "Size-Exclusion Chromatography-based isolation minimally alters Extracellular Vesicles' characteristics compared to precipitating agents," *Sci Rep*, vol. 6, no. 1, Art. no. 1, Sep. 2016, doi: 10.1038/srep33641.
[60] J. Lötvall *et al.*, "Minimal experimental requirements for definition of extracellular vesicles and their functions: a position statement from the International Society for Extracellular Vesicles," *J Extracell Vesicles*, vol. 3, p. 10.3402/jev.v3.26913, Dec. 2014, doi: 10.3402/jev.v3.26913.
[61] F. J. Verweij *et al.*, "The power of imaging to understand extracellular vesicle biology in vivo," *Nat Methods*, vol. 18, no. 9, pp. 1013–1026, Sep. 2021, doi: 10.1038/s41592-021-01206-3.
[62] Y. Yuana, J. Levels, A. Grootemaat, A. Sturk, and R. Nieuwland, "Co-isolation of extracellular vesicles and high-density lipoproteins using density gradient ultracentrifugation," *J Extracell Vesicles*, vol. 3, p. 10.3402/jev.v3.23262, Jul. 2014, doi: 10.3402/jev.v3.23262.

[63] J. Van Deun *et al.*, “Integrated dual-mode chromatography to enrich extracellular vesicles from plasma,” *Adv Biosyst*, vol. 4, no. 12, p. e1900310, Dec. 2020, doi: 10.1002/adbi.201900310.
[64] H. Shao, H. Im, C. M. Castro, X. Breakefield, R. Weissleder, and H. Lee, “New Technologies for Analysis of Extracellular Vesicles,” *Chem. Rev.*, vol. 118, no. 4, pp. 1917–1950, Feb. 2018, doi: 10.1021/acs.chemrev.7b00534.
[65] P. Pužar Dominkuš *et al.*, “PKH26 labeling of extracellular vesicles: Characterization and cellular internalization of contaminating PKH26 nanoparticles,” *Biochimica et Biophysica Acta (BBA) - Biomembranes*, vol. 1860, no. 6, pp. 1350–1361, Jun. 2018, doi: 10.1016/j.bbamem.2018.03.013.
[66] M. Collot *et al.*, “MemBright: A Family of Fluorescent Membrane Probes for Advanced Cellular Imaging and Neuroscience,” *Cell Chemical Biology*, vol. 26, no. 4, pp. 600-614.e7, Apr. 2019, doi: 10.1016/j.chembiol.2019.01.009.
[67] J. H. Holgate and J. Webb, “MICROSCOPY | Light Microscopy and Histochemical Methods,” in *Encyclopedia of Food Sciences and Nutrition*, Elsevier, 2003, pp. 3917–3922. doi: 10.1016/B0-12-227055-X/00778-1.
[68] E. H. K. Stelzer, “Beyond the diffraction limit?,” *Nature*, vol. 417, no. 6891, Art. no. 6891, Jun. 2002, doi: 10.1038/417806a.
[69] V. Gurtler, Ed., *Fluorescent probes*, First edition. in Methods in microbiology, no. volume 48. London Oxford San Diego, CA Cambridge, MA: Academic Press, 2021.
[70] L. Schermelleh *et al.*, “Super-resolution microscopy demystified,” *Nat Cell Biol*, vol. 21, no. 1, Art. no. 1, Jan. 2019, doi: 10.1038/s41556-018-0251-8.
[71] F. Chen, P. W. Tillberg, and E. S. Boyden, “Expansion Microscopy,” *Science*, vol. 347, no. 6221, pp. 543–548, Jan. 2015, doi: 10.1126/science.1260088.
[72] P. Tillberg, “Protein-retention expansion microscopy: Improved sub-cellular imaging resolution through physical specimen expansion,” in *Methods in Cell Biology*, Elsevier, 2021, pp. 1–14. doi: 10.1016/bs.mcb.2020.04.015.
[73] P. W. Tillberg *et al.*, “Protein-retention expansion microscopy of cells and tissues labeled using standard fluorescent proteins and antibodies,” *Nat Biotechnol*, vol. 34, no. 9, Art. no. 9, Sep. 2016, doi: 10.1038/nbt.3625.
[74] T. J. Chozinski *et al.*, “Expansion microscopy with conventional antibodies and fluorescent proteins,” *Nat Methods*, vol. 13, no. 6, Art. no. 6, Jun. 2016, doi: 10.1038/nmeth.3833.
[75] A. T. Wassie, Y. Zhao, and E. S. Boyden, “Expansion microscopy: principles and uses in biological research,” *Nat Methods*, vol. 16, no. 1, Art. no. 1, Jan. 2019, doi: 10.1038/s41592-018-0219-4.
[76] H. Kolesová, V. Olejníčková, A. Kvasilová, M. Gregorovičová, and D. Sedmera, “Tissue clearing and imaging methods for cardiovascular development,” *iScience*, vol. 24, no. 4, p. 102387, Apr. 2021, doi: 10.1016/j.isci.2021.102387.
[77] B. R. Gallagher and Y. Zhao, “Expansion microscopy: A powerful nanoscale imaging tool for neuroscientists,” *Neurobiology of Disease*, vol. 154, p. 105362, Jul. 2021, doi: 10.1016/j.nbd.2021.105362.
[78] Y. Zhao *et al.*, “Nanoscale imaging of clinical specimens using pathology-optimized expansion microscopy,” *Nat Biotechnol*, vol. 35, no. 8, Art. no. 8, Aug. 2017, doi: 10.1038/nbt.3892.
[79] L. Yang, Y. Huang, Z. Zhang, Y. Han, and C. Kuang, “Multicolor expansion fluorescence emission difference microscopy to reveal potential organelle contacts,” *Optics Communications*, vol. 520, p. 128474, Oct. 2022, doi: 10.1016/j.optcom.2022.128474.

[80] D. Jurriens, V. van Batenburg, E. A. Katrukha, and L. C. Kapitein, "Mapping the neuronal cytoskeleton using expansion microscopy," in *Methods in Cell Biology*, Elsevier, 2021, pp. 105–124. doi: 10.1016/bs.mcb.2020.04.018.

[81] F. Chen *et al.*, "Nanoscale imaging of RNA with expansion microscopy," *Nat Methods*, vol. 13, no. 8, Art. no. 8, Aug. 2016, doi: 10.1038/nmeth.3899.

[82] J. S. Holsapple *et al.*, "Expansion microscopy of neutrophil nuclear structure and extracellular traps," *Biophysical Reports*, vol. 3, no. 1, p. 100091, Mar. 2023, doi: 10.1016/j.bpr.2022.100091.

[83] R. Devi, L. Pelletier, and S. L. Prosser, "Charting the complex composite nature of centrosomes, primary cilia and centriolar satellites," *Current Opinion in Structural Biology*, vol. 66, pp. 32–40, Feb. 2021, doi: 10.1016/j.sbi.2020.10.006.

[84] J. Menezes, W. Leibold, G. Klein, and G. Clements, "Establishment and characterization of an Epstein-Barr virus (EBC)-negative lymphoblastoid B cell line (BJA-B) from an exceptional, EBV-genome-negative African Burkitt's lymphoma," *Biomedicine*, vol. 22, no. 4, pp. 276–284, Jul. 1975.

[85] M. A. Epstein, B. G. Achong, Y. M. Barr, B. Zajac, G. Henle, and W. Henle, "Morphological and virological investigations on cultured Burkitt tumor lymphoblasts (strain Raji)," *J Natl Cancer Inst*, vol. 37, no. 4, pp. 547–559, Oct. 1966.

[86] G. Wen *et al.*, "Evaluation of Direct Grafting Strategies via Trivalent Anchoring for Enabling Lipid Membrane and Cytoskeleton Staining in Expansion Microscopy," *ACS Nano*, vol. 14, no. 7, pp. 7860–7867, Jul. 2020, doi: 10.1021/acsnano.9b09259.

[87] F. U. Zwettler *et al.*, "Molecular resolution imaging by post-labeling expansion single-molecule localization microscopy (Ex-SMLM)," *Nat Commun*, vol. 11, no. 1, Art. no. 1, Jul. 2020, doi: 10.1038/s41467-020-17086-8.

[88] G. Wen, V. Leen, Y. Jia, T. Rohand, and J. Hofkens, "Improved Dye Survival in Expansion Microscopy through Stabilizer-Conjugated Linkers," *Chemistry – A European Journal*, vol. 28, no. 66, p. e202202404, 2022, doi: 10.1002/chem.202202404.

[89] A. F. Hill, "Extracellular Vesicles and Neurodegenerative Diseases," *J. Neurosci.*, vol. 39, no. 47, pp. 9269–9273, Nov. 2019, doi: 10.1523/JNEUROSCI.0147-18.2019.

[90] S. Rome, A. Forterre, M. L. Mizgier, and K. Bouzakri, "Skeletal Muscle-Released Extracellular Vesicles: State of the Art," *Frontiers in Physiology*, vol. 10, 2019, Accessed: Mar. 19, 2023. [Online]. Available: https://www.frontiersin.org/articles/10.3389/fphys.2019.00929

[91] M. Mathieu *et al.*, "Specificities of exosome versus small ectosome secretion revealed by live intracellular tracking of CD63 and CD9," *Nat Commun*, vol. 12, no. 1, Art. no. 1, Jul. 2021, doi: 10.1038/s41467-021-24384-2.

[92] Y. Wu *et al.*, "Three-dimensional virtual refocusing of fluorescence microscopy images using deep learning," *Nat Methods*, vol. 16, no. 12, Art. no. 12, Dec. 2019, doi: 10.1038/s41592-019-0622-5.

[93] J. W. Pylvänäinen *et al.*, "Fast4DReg - fast registration of 4D microscopy datasets," *J Cell Sci*, vol. 136, no. 4, p. jcs260728, Feb. 2023, doi: 10.1242/jcs.260728.

[94] S. M. Asano, R. Gao, A. T. Wassie, P. W. Tillberg, F. Chen, and E. S. Boyden, "Expansion Microscopy: Protocols for Imaging Proteins and RNA in Cells and Tissues," *Current Protocols in Cell Biology*, vol. 80, no. 1, p. e56, 2018, doi: 10.1002/cpcb.56.

[95] "EV Profiler Kit," *ONI*. https://oni.bio/nanoimager/reagents-consumables/ev-profiler/ (accessed Mar. 27, 2023).

[96] C. Théry *et al.*, "Minimal information for studies of extracellular vesicles 2018 (MISEV2018): a position statement of the International Society for Extracellular Vesicles and update of the MISEV2014 guidelines," *J Extracell Vesicles*, vol. 7, no. 1, p. 1535750, Nov. 2018, doi: 10.1080/20013078.2018.1535750.

[97] H. G. J. Damstra *et al.*, "GelMap: Intrinsic calibration and deformation mapping for expansion microscopy." bioRxiv, p. 2022.12.21.521394, Dec. 22, 2022. doi: 10.1101/2022.12.21.521394.

[98] N. Korvenlaita *et al.*, "Dynamic release of neuronal extracellular vesicles containing miR-21a-5p is induced by hypoxia," *Journal of Extracellular Vesicles*, vol. 12, no. 1, p. 12297, 2023, doi: 10.1002/jev2.12297.